www.sciencemag.org/cgi/content/full/science.1192160/DC1

Supporting Online Material for

# Ultra-High Porosity in Metal-Organic Frameworks

Hiroyasu Furukawa, Nakeun Ko, Yong Bok Go, Naoki Aratani, Sang Beom Choi, Eunwoo Choi, A. Özgür Yazaydin, Randall Q. Snurr, Michael O'Keeffe, Jaheon Kim,* Omar M. Yaghi*

*To whom correspondence should be addressed. E-mail: jaheon@ssu.ac.kr (J.K.); yaghi@chem.ucla.edu (O.M.Y.)

Published 1 July 2010 on *Science* Express
DOI: 10.1126/science.1192160

**This PDF file includes:**

Supporting Online Material for

# Ultra-High Porosity in Metal-Organic Frameworks

Hiroyasu Furukawa,[1] Nakeun Ko,[2] Yong Bok Go,[1] Naoki Aratani,[1] Sang Beom Choi,[2] Eunwoo Choi,[1] A. Özgür Yazaydin,[3] Randall Q. Snurr,[3] Michael O'Keeffe,[1] Jaheon Kim,[2]* Omar M. Yaghi[1]*

[1]Center for Reticular Chemistry at the California NanoSystems Institute, and Department of Chemistry and Biochemistry, University of California-Los Angeles, 607 East Charles E. Young Drive, Los Angeles, CA 90095, USA. [2]Department of Chemistry, Soongsil University, Seoul 156-743, Korea. [3]Department of Chemical and Biological Engineering, Northwestern University, Evanston, IL 60208, USA.

To whom correspondence should be addressed. E-mail: jaheon@ssu.ac.kr (J.K.); yaghi@chem.ucla.edu (O.M.Y.)

**This PDF file includes:**

# Table of Contents

## **Section S1** Syntheses of Materials

**METHODS:**

**Chemicals used in this work:**

2,6-Naphthalendicarboxylic acid ($H_2$NDC), biphenyl-4,4′-dicarboxylic acid ($H_2$BPDC), zinc(II) nitrate hexahydrate ($Zn(NO_3)_2 \cdot 6H_2O$), and anhydrous acetone were purchased from Sigma-Aldrich Co. and *N*,*N*-dimethylformamide (DMF) and 1-methyl-2-pyrrolidinone (NMP) were purchased from Fisher Scientific International Inc. Zinc(II) nitrate tetrahydrate ($Zn(NO_3)_2 \cdot 4H_2O$) was purchased from EM Science. Pyridine was purchased from Daejung Chemicals & Metals Co., Ltd. All starting materials except for *N*,*N*-diethylformamide (DEF, BASF) were used without further purifications. DEF was treated by addition of charcoal carbon (*ca.* 0.5 g, Acros, CAS No.: 7440-44-0) into 1 L and stirred 12 h at room temperature. The black suspension solution was filtered through a silica-gel column (*ca.* 350 g, Silica gel 60, 230-400 mesh, EMD Chemicals) to remove carbon powder. 1,3,5-Tris(4′-carboxyphenyl-)benzene ($H_3$BTB) was prepared according to published procedures (*S1*).

**Syntheses of organic linkers:**

**A. 4,4',4''-(Benzene-1,3,5-triyltris(ethyne-2,1-diyl))tribenzoic acid ($H_3$BTE)** (*S2-S5*)

**Trimethyl 4,4',4''-(benzene-1,3,5-triyltris(ethyne-2,1-diyl))tribenzoate.** A mixture of methyl 4-iodobenzoate (2.29 g, 8.75 mmol), $Pd(PPh_3)_2Cl_2$ (154 mg, 0.22 mmol) and CuI (209 mg, 1.10 mmol) in $NEt_3$ (30 mL) was added to 1,3,5-triethynylbenzene (365 mg, 2.43 mmol) in $NEt_3$ (10 mL). The mixture was stirred for 20 h at room temperature under argon atmosphere. The solution was evaporated and the residue was dissolved in $CH_2Cl_2$. The organic layer was washed by brine, dried over $MgSO_4$, filtered and concentrated. Purification of the crude product by flash column chromatography on silica gel ($CH_2Cl_2$) provided trimethyl 4,4',4''-(benzene-1,3,5-triyltris(ethyne-2,1-diyl))tribenzoate as a pale yellow powder (788 mg, 59%): mp 177 °C; $^1$H-NMR ($CDCl_3$, 400 MHz) δ 8.05 (d, 6H, $J$ = 8.4 Hz), 7.70 (s, 3H), 7.60 (d, 6H, $J$ = 8.4 Hz), 3.94 (s, 9H); $^{13}$C-NMR ($CDCl_3$, 100 MHz) δ 166.5, 134.6, 131.6, 130.0 129.6, 127.3, 123.8, 90.3, 90.0, 52.3; FT-IR (KBr, 4000-400 $cm^{-1}$) 3428 (br), 2951 (w), 2372 (w), 1724 (s), 1604 (S), 1435 (m), 1403 (w), 1274 (s), 1175 (m), 1105 (s), 1017 (w), 857 (w), 768 (s).

**4,4',4''-(Benzene-1,3,5-triyltris(ethyne-2,1-diyl))tribenzoic acid.** A mixture of trimethyl 4,4',4''-(benzene-1,3,5-triyltris(ethyne-2,1-diyl))tribenzoate (773 mg, 1.40 mmol), $LiOH \cdot H_2O$ (881 mg, 21.0 mmol), tetrahydrofuran (THF, 25 mL) and water (5 mL) was stirred for 16 h at room temperature. The reaction mixture was concentrated. The residue was acidified with cold 3 M HCl (1 M = 1 mol $dm^{-3}$) and cooled in an ice bath. The precipitate was filtered and washed with cold 3 M HCl. The ivory solid was dried. The dried solid was taken up in THF and filtered to remove insoluble inorganic salt. The solution was dried over $MgSO_4$, filtered concentrated and dried under vacuum to give an ivory solid (693 mg, 97%): mp 352 °C; $^1$H-NMR (DMSO-$d_6$, 400 MHz) δ 8.01 (d, 6H, $J$ = 8.0 Hz), 7.88 (s, 3H), 7.72 (d, 6H, $J$ = 8.0 Hz); $^{13}$C-NMR (DMSO-$d_6$, 100 MHz) δ 166.6, 134.5, 131.8, 131.0 129.6, 126.0, 123.4, 90.3, 89.8; FT-IR (KBr, 4000-400 $cm^{-1}$) 3428 (br), 2994 (br), 2658 (w), 2534 (w), 2376 (w), 1687 (s), 1604 (s), 1518 (s), 1312 (s), 1277 (s), 1173 (w), 1105 (w), 856 (m), 768 (s); MALDI-TOF MS ($m/z$) $[M]^+$ 510.0935 (found), 510.1103 (calcd. for $C_{33}H_{18}O_6$).

**B. 4,4',4''-(Benzene-1,3,5-triyl-tris(benzene-4,1-diyl))tribenzoic acid ($H_3$BBC)** (*S6*, *S7*)

**Trimethyl 4,4',4''-(benzene-1,3,5-triyl-tris(benzene-4,1-diyl))tribenzoate.** Anhydrous 1,2-dimethoxyethane (150 mL) was placed in a two-neck 250-mL round bottom flask equipped with a magnetic stirring bar and a reflux condenser under nitrogen atmosphere. 4-Methoxycarbonylphenylboronic acid (2.98 g, 16.6 mmol), CsF (5.03 g, 33.1 mmol), $Pd(PPh_3)_4$ (574 mg, 0.50 mmol), and 1,3,5-tris(4-bromo-phenyl)benzene (2.00 g, 3.68 mmol) were added to the flask, and the reaction mixture was refluxed for 48 h under nitrogen atmosphere. The solution was cooled to room temperature and evaporated under vacuum. The residue was dissolved in $CHCl_3$, washed with water and dried over $MgSO_4$. The solvent was evaporated under vacuum. Further purification was achieved by dissolving the product in 50 mL of diethyl ether and the solution was heated for 20 min and placed in the refrigerator for 1 h. The white product was collected by filtration and dried in vacuum overnight (2.1 g, 80%): mp 218 °C; $^1$H-NMR ($CDCl_3$, 400 MHz) δ 8.17 (d, 6H, $J$ = 8.0Hz), 7.93 (s, 3H), 7.86 (d, 6H, $J$ = 8.4Hz), 7.80 (d, 6H, $J$ = 8.4Hz), 7.77 (d, 6H, $J$ = 8.4Hz), 3.90 (s, 9H); $^{13}$C-NMR ($CDCl_3$, 100 MHz) δ 167.4, 145.4, 142.3, 141.1, 139.7, 130.6, 129.5, 128.3, 128.2, 127.4, 125.6, 52.6; FT-IR (KBr, 4000-400 $cm^{-1}$) 3428 (br), 2947 (w), 1932 (w), 1719 (s), 1607 (m), 1434 (m), 1277 (s), 1180 (m), 1110 (s), 1004 (m), 824 (s), 772 (s).

**4,4',4''-(Benzene-1,3,5-triyl-tris(benzene-4,1-diyl))tribenzoic acid.**

Trimethyl 4,4',4''-(benzene-1,3,5-triyl-tris(benzene-4,1-diyl))tribenzoate (2.00 g, 2.82 mmol), 2.2 g of NaOH, THF, water, and methanol (200, 80, and 50 mL, respectively) were mixed in a 1 L round bottom flask equipped with a magnetic stirring bar, and the mixture was stirred for 2 days at room temperature. The solution was evaporated under vacuum. The residue was acidified with 3 M HCl. The white solid was collected by filtration, washed with methylene chloride and methanol and dried in vacuum overnight (1.80 g, 96%): mp 326 °C; $^{1}$H-NMR (DMSO-$d_6$, 400 MHz) δ 13.07 (br, 3H) 8.07 (d, 6H, $J$ = 8.0Hz), 8.06 (s, 3H), 8.05 (d, 6H, $J$ = 8.0Hz), 7.91 (d, 6H, $J$ = 7.6Hz), 7.89 (d, 6H, $J$ = 7.2Hz); $^{13}$C-NMR (DMSO-$d_6$, 100 MHz) δ 168.0, 144.6, 141.9, 140.7, 139.2, 130.9, 130.6, 128.8, 128.4, 127.6, 125.3; FT-IR (KBr, 4000-400 cm$^{-1}$) 3448 (br), 3029 (br), 2661 (w), 2536 (w), 1925 (w), 1686 (s), 1606 (s), 1419 (m), 1276 (m), 1177 (m), 1118 (m), 1003 (m), 824 (s), 773 (s); MALDI-TOF MS ($m/z$) [M]$^{+}$ 666.2976 (found), 666.2042 (calcd. for $C_{45}H_{30}O_6$).

**Analytical techniques**: Single-crystal X-ray diffraction data for MOF-200 were collected at 100 K using a Bruker Platium 200 diffractometer with synchrotron radiation (λ = 0.77490 Å) at Beamline 11.3.1 at the Advanced Light Source (ALS), Lawrence Berkeley National Laboratory. Single-crystal X-ray diffraction data for MOF-205 and MOF-210 were collected at 100 K using synchrotron radiation (λ = 0.90000 Å (MOF-205), and 1.10000 Å (MOF-210), respectively) at beamlines 4A HFMX, and 6B MX-I, Pohang Accelerator Laboratory (PAL) in Korea. The diffraction data for MOF-180 were collected at 258 K on a Bruker APEX CCD diffractometer with CuKα (λ = 1.54178 Å). Powder X-ray diffraction data were collected using a Bruker D8 Discover $\theta$–$2\theta$ diffractometer in reflectance Bragg–Brentano geometry at 40 kV, 40 mA (1,600 W) for CuK$\alpha_1$ radiation (λ = 1.5406 Å) (SOM, Section S3). TGA was carried out using a TA Q500 and a Scinco TGA-S1000 thermal analysis system (SOM, Section S5). Fourier-transform infrared spectra (FT-IR) of samples prepared as KBr pellets were measured using a Nicolet FT-IR Impact 400 system and a JASCO FT/IR-4000 spectrophotometer.

**Synthesis and characterization of MOFs:**

**MOF-180.** A solid mixture of $H_3BTE$ (7.5 mg, 0.015 mmol) and $Zn(NO_3)_2{\cdot}6H_2O$ (75 mg, 0.25 mmol) was dissolved in a mixture of DMF/NMP (2.0/2.0 mL) in an 8-mL glass vial. The clear reaction solution was heated in an isotherm oven at 85 °C for 96 h resulting in colorless polyhedral crystals, which were isolated by washing with a mixture of DMF and NMP (3 × 4 mL) and dried in air. Yield: 5.2 mg, 27% based on 1 mol of $H_3BTE$. Elemental microanalysis for $Zn_4O(BTE)_2(H_2O)_3{\cdot}H_2O \equiv C_{66}H_{32}O_{14}Zn_4$, calculated (%): C, 60.49; H, 2.46; N, 0.00. Found (%): C, 60.98; H, 2.54; N, 0.06. FT-IR (KBr, 4000-400 $cm^{-1}$): 3422 (br, w), 1604 (s), 1534 (s), 1413 (vs), 1176 (w), 1016 (w), 875 (w), 859 (m), 779 (s), 743 (w), 698 (w), 677 (w), 609 (w), 523 (w), 446 (w), 405 (w).

**MOF-200.** A solid mixture of $H_3BBC$ (22.0 mg, 0.033 mmol) and $Zn(NO_3)_2{\cdot}6H_2O$ (98.2 mg, 0.33 mmol) was dissolved in a mixture of DEF/NMP (4.0/4.0 mL) in a 20-mL glass vial. The clear reaction solution was heated in an isotherm oven at 85 °C for 24 h resulting in colorless trigonal prismatic crystals, which were isolated by washing with a mixture of DEF and NMP (3 × 4 mL) and dried in air. Yield: 30 mg, 29% based on 1 mol of $H_3BBC$. Elemental microanalysis for $Zn_4O(BBC)_2(H_2O)_3{\cdot}H_2O \equiv C_{90}H_{62}O_{17}Zn_4$, calculated (%): C, 64.46; H, 3.73; N, 0.00. Found (%): C, 64.42; H, 3.57; N, 0.00. FT-IR (KBr, 4000-400 $cm^{-1}$): 1928 (w), 1800 (w), 1709 (m), 1612 (vs), 1566 (s), 1525 (s), 1408 (vs), 1184 (m), 1108 (w), 1006 (m), 869 (w), 828 (s), 787 (s), 706 (w), 655 (m), 558 (w), 512 (w).

**MOF-200 (large scale synthesis).** A solid mixture of $H_3BBC$ (200 mg, 0.30 mmol) and $Zn(NO_3)_2{\cdot}6H_2O$ (950 mg, 3.19 mmol) was dissolved in a mixture of DEF/NMP (80/80 mL) in a 500-mL Nalgene® high-density polyethylene (HDPE) container. Reaction solution was sonicated for 1 h prior to heating, and then placed in an isothermal oven at 82 °C for 48 h to give the crystals of MOF-200 (150 - 170 mg, 44 - 50% yield based on 1 mol of $H_3BBC$).

**MOF-205.** A solid mixture of $H_3BTB$ (12.8 mg, 0.029 mmol), and $H_2NDC$ (10.5 mg, 0.049 mmol), and $Zn(NO_3)_2{\cdot}6H_2O$ (42.5 mg, 0.14 mmol) was dissolved in a mixture of DMF/EtOH (3.0/0.3 mL) in a 4-mL vial. The vial was capped and heated in an isothermal oven at 95 °C for 24 h to give colorless truncated-octahedral crystals. The reaction mixture was allowed to cool naturally to room temperature and the crystals were washed with DMF and dried in air. Yield: 21 mg, 68% based on 1 mol of $H_3BTB$. Elemental

microanalysis for MOF-205, $Zn_4O(BTB)_{4/3}(NDC) \equiv C_{48}H_{26}O_{13}Zn_4$, calculated (%): C, 53.78; H, 2.48; N, 0.00. Found (%): C, 53.58; H, 2.29; N, < 0.1. FT-IR (KBr, 4000-400 $cm^{-1}$): 3335 (s, br), 1584 (vs), 1541 (vs), 1406 (vs), 1186 (m), 1141 (w), 1108 (w), 1015 (w), 921 (w), 854 (m), 779 (vs), 704 (m), 672 (w), 560 (w), 475 (m), 457 (m), 442 (m), 419 (w).

**MOF-210.** A solid mixture of $H_3BTE$ (8.3 mg, 0.016 mmol), $H_2BPDC$ (15.7 mg, 0.065 mmol), and $Zn(NO_3)_2 \cdot 6H_2O$ (42.5 mg, 0.14 mmol) was dissolved in a mixture of DMF/NMP (5.0/5.0 mL) in a 20-mL vial. The vial was capped and heated in an isothermal oven at 95 °C for 72 h to give colorless polyhedral crystals. The reaction mixture was allowed to cool naturally to room temperature and the crystals were washed with DMF and dried in air. Yield: 13 mg, 68% based on 1 mol of $H_3BTE$. Elemental microanalysis for MOF-210, $Zn_4O(BTE)_{4/3}(BPDC) \equiv C_{58}H_{28}O_{13}Zn_4$, calculated based on framework only (%): C, 53.78; H, 2.48; N, 0.00. Found (%): C, 53.58; H, 2.29; N, < 0.1. FT-IR (KBr, 4000-400 $cm^{-1}$): 3338 (s, br), 2206 (w), 1934 (w), 1654 (w), 1604 (vs), 1579 (vs), 1533 (vs), 1407 (vs), 1175 (m), 1098 (w), 1015 (w), 960 (w), 859 (m), 770 (s), 744 (w), 699 (w), 679 (w), 607 (w), 526 (w), 471 (w), 456 (m), 439 (m), 419 (m).

## **Section S2** Single Crystal X-ray Diffraction Analyses

**MOF-180.** A colorless polyhedral crystal was sealed in a capillary, and its diffraction data set was collected at 258 K on a Bruker APEX CCD diffractometer with CuKα radiation (λ = 1.54178 Å). Bruker SMART program (*S8*) was used for data collection, and SAINT (*S9*) was used for cell refinement, and reduction. Absorption correction was applied using SADABS (*S10*). XPREP suggested a trigonal space group, $P\bar{3}1c$ (No. 163) with a CFOM of 7.99. Since the space group is the same as MOF-177 ($Zn_4O(BTB)_2$) (*S11*), it is expected that the atomic connectivity of MOF-180 is also similar with that of MOF-177 (the **qom** net). Due to the weak diffraction intensities and low resolution (2.23 Å), only the Zn ions could be found. However, this resolution was sufficient for dissolving the Zn···Zn separation in a $Zn_4O$ unit (about 3.2 Å) although it was not for other bonds involving light atoms such as C□O and C□C as well as Zn□O bonds (~ 2.0 Å). In more detail, direct methods by XS in SHELX-TL software package (*S12*) suggested two unique Zn atoms (Zn1 and Zn2) belonging to one of two independent $Zn_4O$ units in the asymmetric unit. The symmetry generated Zn atoms formed a tetrahedral arrangement with inter-atomic distances of about 3.4 Å. The third Zn atom examination on the electron density maps by WinGX (*S13*) indicated that a moiety of large electron densities was present around a special position (0.3333, 0.6667, 0.2500), which was ascribed to the other $Zn_4O$ unit showing a disorder over two sites. Two oxygen atoms (O1C and O2C) were generated at the centers of the two $Zn_4O$ moieties; O1C and O2C sit on Wyckoff positions *h* and *d*, respectively. All the Zn atoms were refined anisotropically with application of restrains on interatomic distances and thermal parameters (DFIX and ISOR instructions in XL). Because of the very low and diffuse residual electron densities, it was not possible to identify the C and O atoms of the organic linkers. However, it was clear that noticeable electron densities were joining $Zn_4O$ moieties and they corresponded to the BTE linkers (Fig. S1). Therefore, using the geometric information of a **qom** net, a model structure was built by incorporation of a BTE fragment into the crystal lattice using Materials Studio (*S14*). The final structural model was obtained by Materials Studio Forcite calculations; both the positions of $Zn_4O$ units and the unit cell parameters were not optimized. Due to the disordered one of two $Zn_4O$ units, the bond geometry involving Zn and O atoms were deviated significantly from the ideal values, and therefore, the disordered Zn sites were finally adjusted manually using Materials Studio Visualizer. A part of the extended structure is in Fig. S2, and crystal and refinement data are given in Table S1. Crystallographic data for MOF-

180 has been deposited into the Cambridge Crystallographic Data Centre under deposition number CCDC 775690.

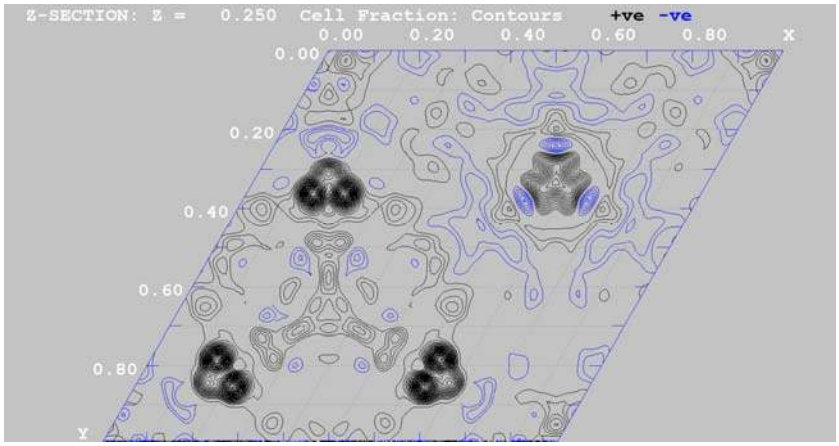


(a)

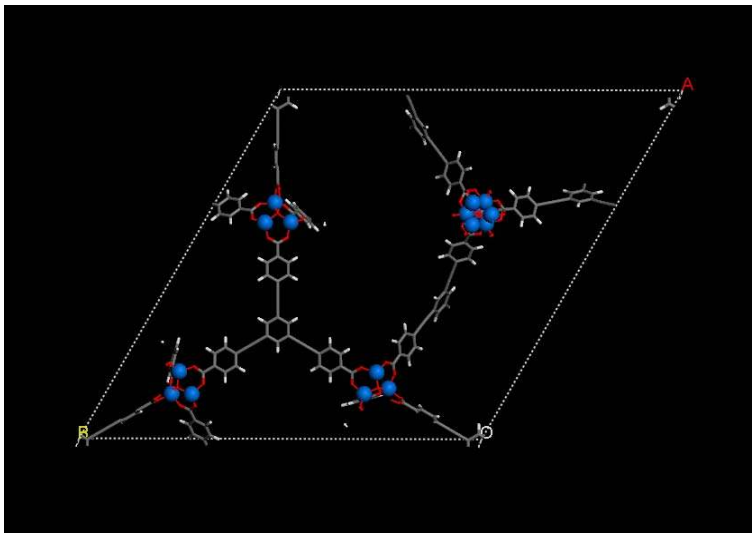


(b)

**Fig. S1.** Selected electron density maps calculated by WinGX FOURIER MAP with $F_0$ coefficients. Sections at (a) $z$ = 0.25 are displayed by WinGX CONTOUR with a contouring level of 0.15 $e^{-}/Å^3$. Black contours are for positive, and blue for negative contours. A model structure is also displayed with a unit cell content of $z = 0 \sim 0.25$ in (b).

**Table S1.** Crystal data and structure refinement for MOF-180. The marked (*) results are based on $Zn_4O$ moieties only.

| | | |
|---|---|---|
| Empirical formula | C66 H30 O13 Zn4 | |
| Formula weight | 1292.38 | |
| Temperature | 258(2) K | |
| Wavelength | 1.54178 Å | |
| Crystal system | Trigonal | |
| Space group | *P*(-3)1*c* | |
| Unit cell dimensions | *a* = 45.846(16) Å | α = 90° |
| | *b* = 45.846(16) Å | β = 90° |
| | *c* = 37.106(25) Å | γ = 120° |
| Volume | 67541(57) $Å^3$ | |
| Z | 8 | |
| Density (calculated) | 0.254 $Mg/m^3$ | |
| Absorption coefficient | 0.415 $mm^{-1}$ | |
| F(000) | 5200 | |
| Crystal size | 0.25 x 0.25 x 0.25 $mm^3$ | |
| Theta range for data collection | 1.11 to 20.20° | |
| Index ranges | -20<=h<=20, -20<=k<=20, -16<=l<=16 | |
| Reflections collected | 31726 | |
| Independent reflections | 2136 [R(int) = 0.0798] | |
| Completeness to theta = 20.20° | 99.8% | |
| Absorption correction | SADABS | |
| Refinement method | Full-matrix least-squares on $F^2$ | |
| *Data / restraints / parameters | 2136 / 37 / 32 | |
| *Goodness-of-fit on $F^2$ | 6.501 | |
| *Final R indices [I>2sigma(I)] | R1 = 0.5843, wR2 = 0.8725 | |
| *R indices (all data) | R1 = 0.6190, wR2 = 0.8965 | |
| *Largest diff. peak and hole | 1.105 and -0.319 e.$Å^{-3}$ | |

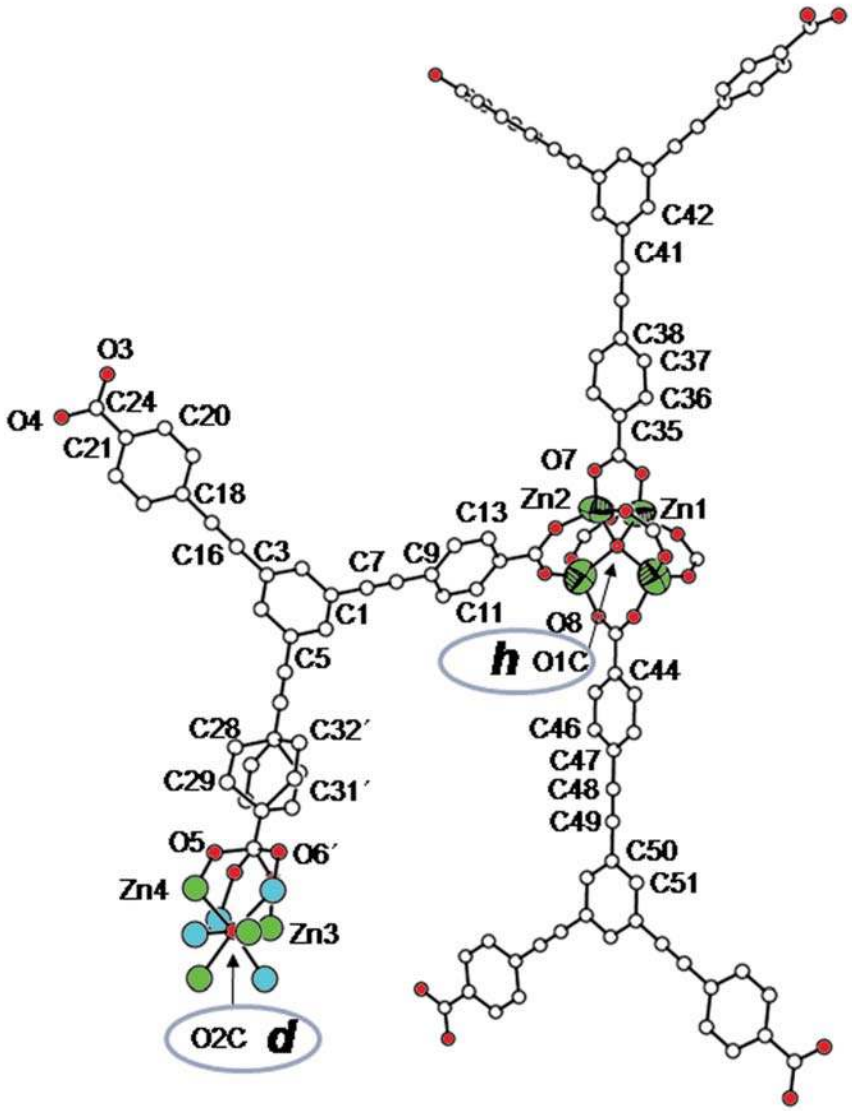


**Fig. S2.** A fragment structure of MOF-180 is displayed by ORTEP. Selected atoms in the asymmetric unit are labeled. A benzene ring (C27 ~ C32) is disordered over two sites at general positions while a $Zn_4O$ unit is disordered at a special position, *d*. According to these disorders, the carboxylate oxygen atoms, O5 and O6 are also disordered over two sites. Thermal ellipsoids for Zn atoms are displayed with 20% probability. Hydrogen atoms are not shown for simplicity.

**MOF-200.** Intensity data were collected at Beamline 11.3.1 at the Advanced Light Source (ALS), Lawrence Berkeley National Laboratory through the SCrALS (Service Crystallography at Advanced Light Source) program. The diffraction data set from a colorless trigonal prismatic crystal sealed in a capillary was collected at 100 K on a Bruker Platinum 200 diffractometer with synchrotron radiation (λ = 0.77490 Å). Bruker APEX-2 program (*S15*) was used for data collection, and SAINT (*S9*) was used for cell refinement, and reduction. Absorption correction was applied using SADABS (*S10*). Crystal structure was solved using SHELX-TL software package (*S12*) with a trigonal space group, $P\bar{3}1c$ (No. 163). An initial model for MOF-200 was obtained by direct methods using XS, and improved by subsequent refinements using XL. Direct methods using a default TREF instruction in XS produced four Zn atoms and many electron density peaks that were difficult to extract ligand. Among four Zn atoms, two Zn atoms, Zn3 and Zn4 showed a statistical disorder over two sites. After fixing their site occupancy factors, and removing all other non-Zn atoms, phase expansion using a TEXP instruction with 2347 $E_0 > 1.5$ was conducted to obtain an improved framework structure. There were three independent BBC links in the asymmetric unit. One lies at a general position and other two at special positions (Wyckoff positions, *a* and *c*, respectively) as shown in Fig. S3). Two independent $Zn_4O$ units were also found at special positions (Wyckoff positions, *d* and *h*, respectively). While a $Zn_4O$ unit at an *h* position is ordered, the other one at a *d* position was disordered over two sites. The latter case required one of three carboxylate groups in the ordered BBC to be present over two positions with a half occupancy. One of the benzene rings of the BBC was also statistically disordered over two sites. Due to tendencies of dynamic disorder of all BBC links, restraints by AFIX, SADI and FLAT instructions were applied to maintain ideal geometry of their aromatic rings. For C43 and C44 atoms, EADP instructions were applied to avoid eccentric thermal ellipsoids. All hydrogen except for coordinating water molecules were placed in calculated positions and refined by applying a riding model. Without including solvent molecules, the refinement converged to R1 = 0.1924, and wR2 = 0.4783 for 12,945 reflections of $I > 2\sigma(I)$. The large volume fraction of disordered solvents was calculated by PALTON SOLV CALC (*S16*) to 88444.1 $Å^3$ which corresponds to 89.2 % of the unit cell volume. PALTON SQUEEZE (*S16*) routine calculated that 10711 electrons per unit cell were attributed to the disordered solvents. With a modified reflection data excluding the solvent contribution, the final refinement process converged to R1 = 0.0686, wR2 = 0.1855 ($I > 2\sigma(I)$). A part of the extended structure is in Fig. S3, and crystal and refinement data are given in Table S2. Crystallographic data for MOF-200 has been

deposited into the Cambridge Crystallographic Data Centre under deposition number CCDC 775691.

**Table S2.** Crystal data and structure refinement for MOF-200.

| | | |
|---|---|---|
| Empirical formula | C90 H60 O16 Zn4 | |
| Formula weight | 1658.86 | |
| Temperature | 100(2) K | |
| Wavelength | 0.77490 Å | |
| Crystal system | Trigonal | |
| Space group | $P\bar{3}1c$ | |
| Unit cell dimensions | $a$ = 52.022(3) Å | α = 90° |
| | $b$ = 52.022(3) Å | β = 90° |
| | $c$ = 42.316(5) Å | γ = 120° |
| Volume | 99176(14) $Å^3$ | |
| Z | 8 | |
| Density (calculated) | 0.222 $Mg/m^3$ | |
| Absorption coefficient | 0.202 $mm^{-1}$ | |
| F(000) | 6784 | |
| Crystal size | 0.30 x 0.30 x 0.20 $mm^3$ | |
| Theta range for data collection | 2.15 to 18.14° | |
| Index ranges | -41<=h<=41, -41<=k<=41, -33<=l<=33 | |
| Reflections collected | 377015 | |
| Independent reflections | 17914 [R(int) = 0.1164] | |
| Completeness to theta = 18.14° | 99.5% | |
| Max. and min. transmission | 0.9607 and 0.9419 | |
| Refinement method | Full-matrix least-squares on $F^2$ | |
| Data / restraints / parameters | 17914 / 387 / 615 | |
| Goodness-of-fit on $F^2$ | 1.051 | |
| Final R indices [I>2sigma(I)] | R1 = 0.0686, wR2 = 0.1855 | |
| R indices (all data) | R1 = 0.0914, wR2 = 0.2005 | |
| Largest diff. peak and hole | 0.253 and -0.321 $e.Å^{-3}$ | |

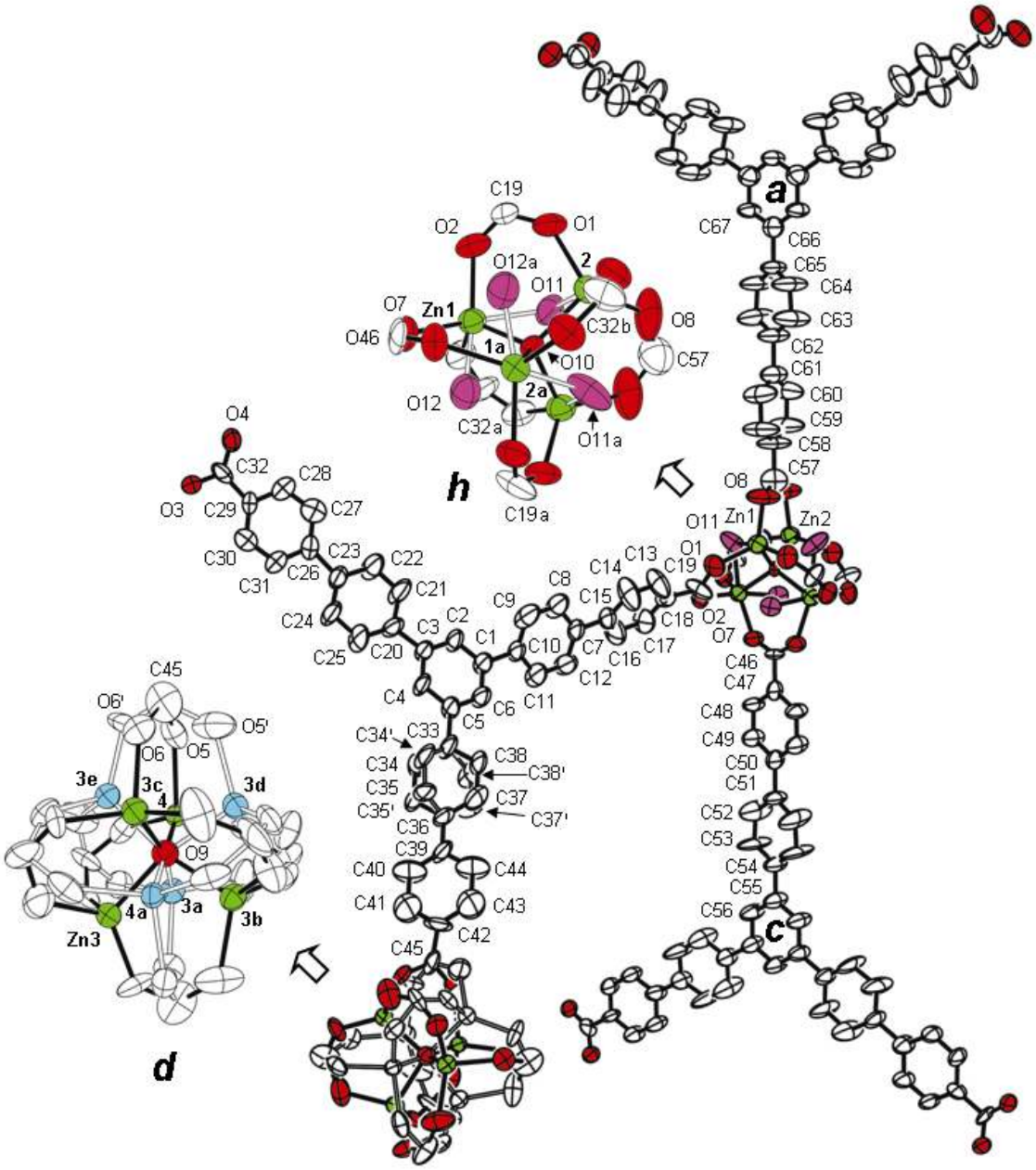


**Fig. S3.** ORTEP drawing (20% probability) of a fragment in MOF-200 is displayed with selected atomic labels. Two BBC and two $Zn_4O$ moieties lie at Wyckoff positions, *a*, *c*, *d*, and *h*. A $Zn_4O$ moiety at *h* has two μ-$H_2O$s and two dangling $H_2O$ which are displayed as pink ellipsoids. The other $Zn_4O$ moiety at *d* is disordered over two sites, which gives two sets of half-occupied Zn atoms denoted with blue and green ellipsoids, respectively.

**MOF-205.** The diffraction data set from a colorless truncated octahedral crystal measuring 0.30 × 0.30 × 0.30 $mm^3$ mounted was collected at 100 K on a ADSC Quantum 210 CCD diffractometer with synchrotron radiation (λ = 0.90000 Å) at Macromolecular Crystallography Wiggler Beamline 4A HFMX, Pohang Accelerator Laboratory (PAL), Pohang, Korea. ADSC Quantum-210 ADX program (Ver. 1.96) (*S17*) was used for data collection. HKL2000 (Ver. 0.98.699) (*S18*) was used for cell refinement, reduction, and absorption correction. Crystal structure was solved using SHELX-TL software package (*S12*) with a cubic space group, $Pm\bar{3}n$ (No. 223). An initial model for MOF-205 was obtained by direct methods using XS, and improved by subsequent refinements using XL. Most non-hydrogen atoms in the framework were easily identified except for a disordered 2,6-naphthalenedicarboxylate (NDC) around a special position (Wyckoff position, *h*). Before resolving the disorder, other atoms were refined anisotropically to suppress noisy electron densities. As the molecular symmetry of NDC ($C_{2h}$ point group or *m*/2 if NDC is flat) is lower than the site symmetry (*mm*2) in the lattice, geometric restraints with DFIX were applied to prevent severe distortion of the naphthalene moiety. In NDC, two terminal carboxylate groups are parallel, but their C atoms not aligned in the same line. This required also a disordered model for the carboxylate. However, further resolution was not been applied, and instead, we have prepared an ordered carboxylate model for simplicity. As it is, the C8 and O3 atoms in the carboxylate have elongated ellipsoids normal to a crystallographic 2-fold rotation axis as shown in Fig. S4. All phenyl groups were refined with restrained models by applying DFIX and FLAT instructions. Hydrogen atoms were placed in calculated positions and refined by applying a riding model. As usually observed in highly porous and symmetric MOF structures, it was very difficult to find occluded solvent molecules from diffuse electron densities. Without including solvent molecules, the refinement converged to R1 = 0.1271, and wR2 = 0.3973 for 4,318 reflections of $I > 2\sigma(I)$. The large volume fraction of disordered solvent was calculated by PALTON SOLV CALC (*S16*) to 23281.0 $Å^3$ which corresponds to 83.3% of the unit cell volume. PALTON SQUEEZE (*S16*) routine calculated that 4551 electrons per unit cell were attributed to the disordered solvents. With a modified reflection data excluding the solvent contribution, the final refinement process converged to R1 = 0.0516, wR2 = 0.1579 ($I > 2\sigma(I)$). A part of the extended structure is displayed in Fig. S4, and crystal and refinement data are given in Table S3. Crystallographic data for MOF-205 has been deposited into the Cambridge Crystallographic Data Centre under deposition number CCDC 775692.

**Table S3.** Crystal data and structure refinement for MOF-205.

| | |
|---|---|
| Empirical formula | C48 H26 O13 Zn4 |
| Formula weight | 1072.17 |
| Temperature | 100(2) K |
| Wavelength | 0.90000 Å |
| Crystal system | Cubic |
| Space group | $Pm\bar{3}n$ |
| Unit cell dimensions | $a$ = 30.353(4) Å $\alpha$ = 90° |
| | $b$ = 30.353(4) Å $\beta$ = 90° |
| | $c$ = 30.353(4) Å $\gamma$ = 90° |
| Volume | 27964(6) $Å^3$ |
| Z | 6 |
| Density (calculated) | 0.382 $Mg/m^3$ |
| Absorption coefficient | 0.524 $mm^{-1}$ |
| F(000) | 3228 |
| Crystal size | 0.30 x 0.30 x 0.30 $mm^3$ |
| Theta range for data collection | 1.70 to 32.37° |
| Index ranges | 0<=h<=36, -36<=k<=36, -36<=l<=36 |
| Reflections collected | 79057 |
| Independent reflections | 4318 [R(int) = 0.0982] |
| Completeness to theta = 32.37° | 98.5% |
| Absorption correction | multi-scan |
| Refinement method | Full-matrix least-squares on $F^2$ |
| Data / restraints / parameters | 4318 / 65 / 99 |
| Goodness-of-fit on $F^2$ | 1.111 |
| Final R indices [I > 2σ(I)] | R1 = 0.0516, wR2 = 0.1579 |
| R indices (all data) | R1 = 0.0583, wR2 = 0.1623 |
| Largest diff. peak and hole | 0.378 and -0.574 $e.Å^{-3}$ |

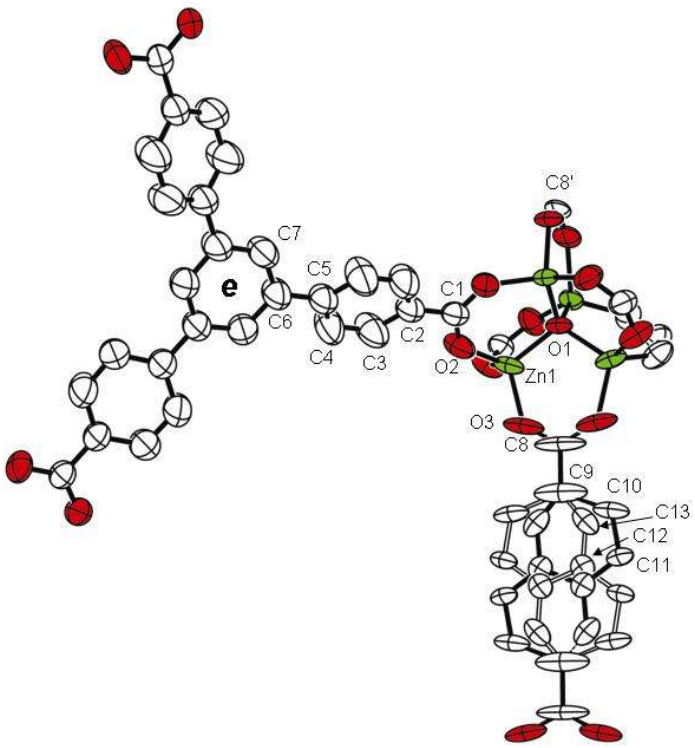


**Fig. S4.** ORTEP drawing (50% probability) of a fragment in MOF-205 is displayed with selected atomic labels. The labeled atoms constitute an asymmetric unit. A tripodal ligand, BTB sits on a special position having site symmetry of 32 (Wyckoff position, *e* at the center of BTB). The central oxo anion, O1 is also located at a special position (Wyckoff *d* position, $\bar{4}m2$ site symmetry). The linear linker, NDC is disordered over two sites due to the crystallographic site symmetry, *mm*2 (Wyckoff position, *h*). Hydrogen atoms are omitted for simplicity. Six points of extension for the inorganic SBU are composed of two NDC carboxylate C atoms (C8 and C8') and the others belonging to four BTB linkers.

**MOF-210.** The diffraction data set from a fragment cut from a twinned crystal measuring 0.35 × 0.30 × 0.25 $mm^3$ mounted was collected at 100 K with synchrotron radiation (λ = 1.10000 Å) on a 6B MX-I ADSC Quantum-210 detector with a silicon (111) double-crystal monochromator at the Pohang Accelerator Laboratory, Korea. The ADSC Quantum-210 ADX program (Ver. 1.96) (*S17*) was used for data collection, and HKL2000 (Ver. 0.98.699) (*S18*) was used for cell refinement, reduction, and absorption correction. Although we mounted more than twenty crystals, the best data has only a low resolution of 1.9 Å, a combinational approach using X-ray crystallography and a structural modeling has been applied to build the structure of MOF-210 similarly to the case of MOF-180. The Zn atoms were found with a trigonal space group, $R\bar{3}$ (No. 148), by direct methods using XS in the SHEX-TL program package (*S12*). Three sets of tetrahedrally-arranged $Zn_4$ clusters were identified and refined anisotropically. The central oxygen atoms were introduced in the center of four Zn atoms per each $Zn_4$ unit. With bond distance restraints using SADI instructions, the geometries of $Zn_4O$ clusters were maintained during refinements. Three central oxygen atoms were also refined anisotropically. At this stage, some oxygen atoms coordinated to Zn atoms were shown in the difference Fourier map. However, incorporation of those atoms could not contribute for the expansion of the structural model. The R1 value was converged to 0.4698 for 9129 observed reflections ($I > 2\sigma(I)$) among 14547 unique reflections. The BTE and BPDC organic linkers were inserted based on both electron density-map analyses and with consideration on the $Zn_4O\cdots Zn_4O$ distances (Fig. S5). Four independent $Zn_4O$ clusters in an asymmetric unit require four BTE and three BPDC links which could be generated using a Materials Studio modeling program. The structural model was finally optimized by the geometry optimization using Materials Studio Forcite routine with fixing both $Zn_4O$ positions and unit cell parameters. The final coordinates were generated in a SHELX ins-file, and further refinements were tried to investigate whether the model would give reduced R-values. However, the refinement processes diverged due to distortion of organic moieties; therefore, refinements with a 'DMAP 0 0' instruction were performed to generate a CIF-file. PLATON ADSYMM (*S16*) indicated the presence of pseudo-symmetry and suggested $R\bar{3}c$ (No. 167) with 88% probability. In fact, the structure could be also solved with $R\bar{3}c$, which gave the same framework connectivity as that for the lower space group, $R\bar{3}$. However, PLATON ADSYMM EXACT (*S16*) calculation supports $R\bar{3}$, and there were many reflections that violated systematic absence conditions in $R\bar{3}c$; 224 reflections (average $I$, 90.0; average $I/\sigma(I)$, 20.9) violated a reflection condition for the $c$-glide plane in $R\bar{3}c$. A part of the extended structure is

shown in Fig. S6, and crystal and refinement data are shown in Table S4. Crystallographic data for MOF-205 has been deposited into the Cambridge Crystallographic Data Centre under deposition number CCDC 775693.

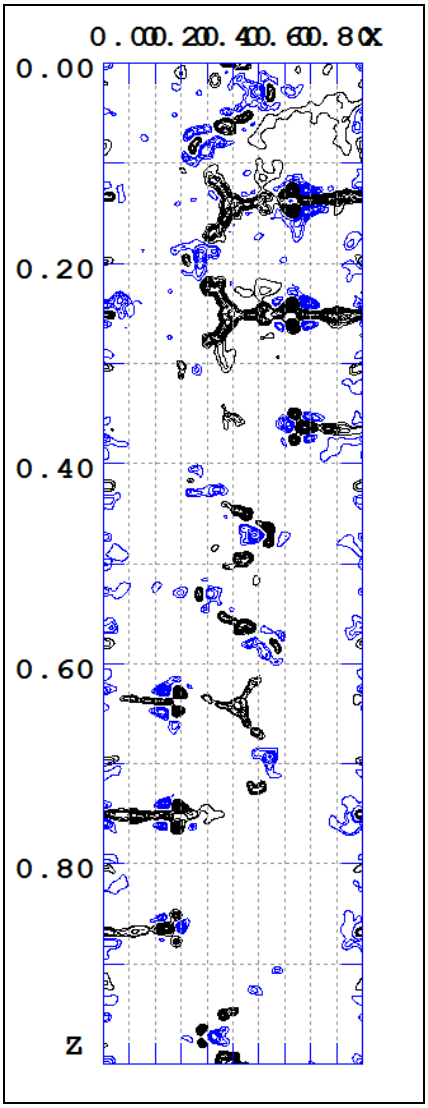


(a)

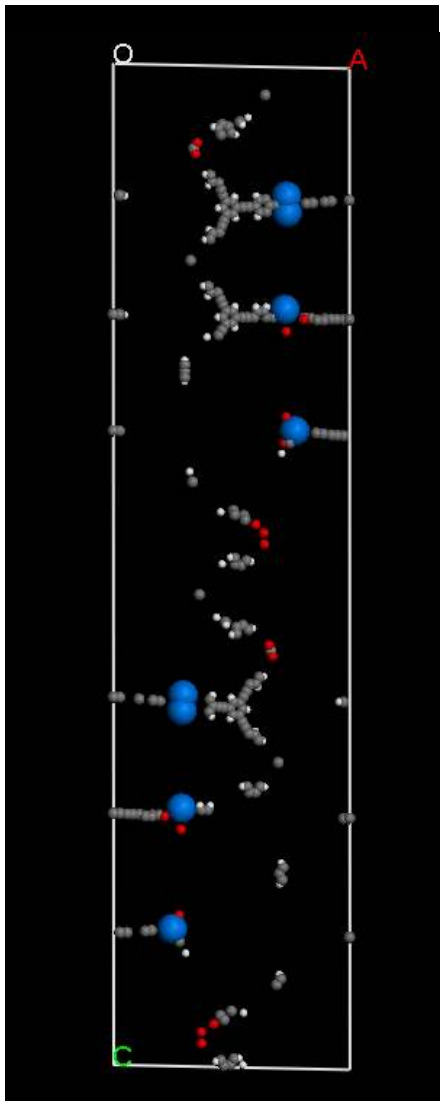


(b)

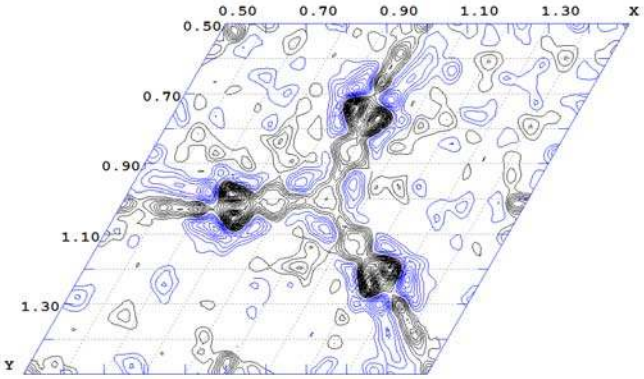


(c)

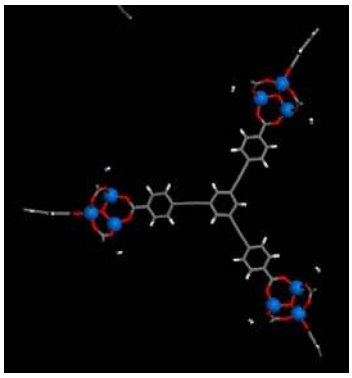

(d)

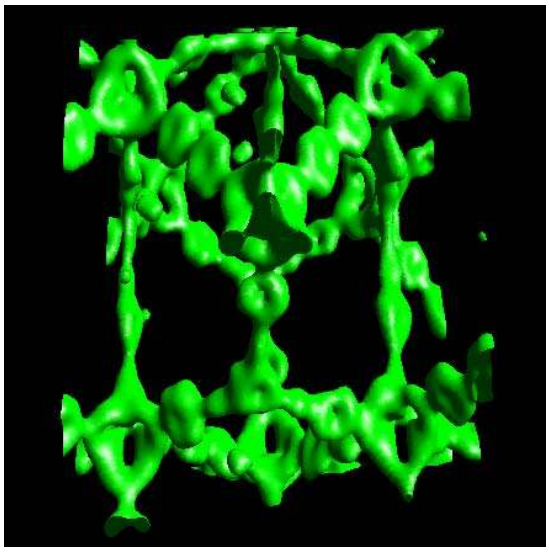

(e)

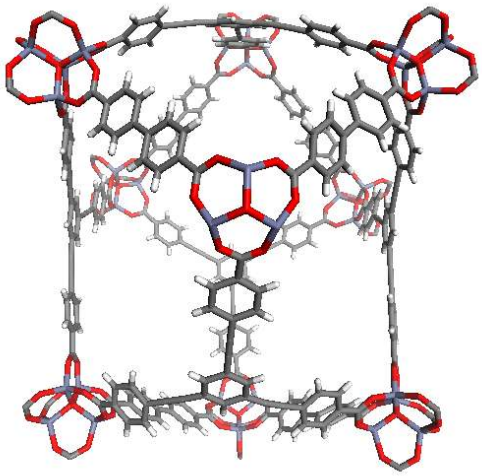

(f)

**Fig. S5.** Selected electron density maps calculated by WinGX FOURIER MAP with $F_0$ coefficients. Sections at (a) $y$ = 0.011, and (c) $z$ = 0.137 are displayed by WinGX CONTOUR with a contouring level of 0.40 $e^-/Å^3$. Black contours are for positive, and blue for negative contours. Structural models at (b) $y$ = 0. ~ 0.03 and (d) $z$ = 0.12 ~ 0.14 are also displayed for comparison with the electron density map. A three-dimensional electron density map in (e) and its corresponding structure in (f) show also BPDC linkers are participating in building MOF-210 framework; the packing range is 0.22 ~ 1.00 for $x$, -0.02 ~ 0.80 for $y$, and 0.05 ~ 0.22 for $z$. The electron density map was drawn by MCE2005 (*S19*).

**Table S4.** Crystal data and structure refinement for MOF-210. The marked (*) results are based on $Zn_4O$ moieties only.

| | | |
|---|---|---|
| Empirical formula | C58 H28 O13 Zn4 | |
| Formula weight | 1194.28 | |
| Temperature | 100(2) K | |
| Wavelength | 1.10000 Å | |
| Crystal system | Trigonal | |
| Space group | $R\bar{3}$ | |
| Unit cell dimensions | $a$ = 50.745(1) Å | α = 90° |
| | $b$ = 50.745(1) Å | β = 90° |
| | $c$ = 194.256(5) Å | γ = 120° |
| Volume | 433203(16) $Å^3$ | |
| Z | 54 | |
| Density (calculated) | 0.247 $Mg/m^3$ | |
| Absorption coefficient | 0.428 $mm^{-1}$ | |
| F(000) | 32400 | |
| Crystal size | 0.35 x 0.30 x 0.25 $mm^3$ | |
| Theta range for data collection | 1.08 to 16.80° | |
| Index ranges | 0<=h<=26, -22<=k<=0, -101<=l<=101 | |
| Reflections collected | 14547 | |
| Independent reflections | 14547 [R(int) = 0.0000] | |
| Completeness to theta = 16.80° | 99.3% | |
| Refinement method | Full-matrix least-squares on $F^2$ | |
| *Data / restraints / parameters | 14547 / 81 / 767 | |
| *Goodness-of-fit on $F^2$ | 4.458 | |
| *Final R indices [I>2sigma(I)] | R1 = 0.4698, wR2 = 0.8118 | |
| *R indices (all data) | R1 = 0.5127, wR2 = 0.8305 | |
| *Largest diff. peak and hole | 0.438 and -0.325 e.$Å^{-3}$ | |

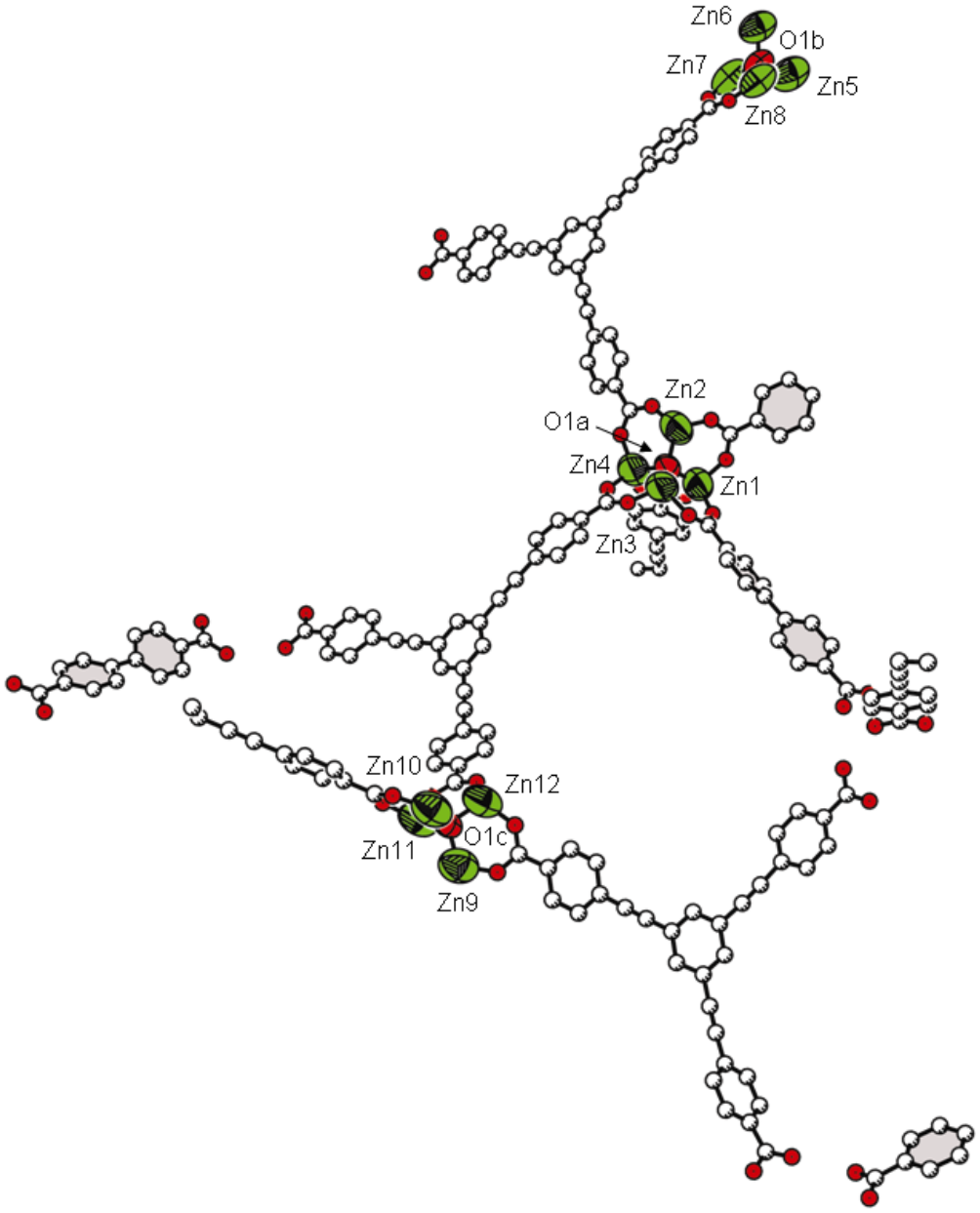


**Fig. S6.** ORTEP drawing of the asymmetric unit for MOF-210. Thermal ellipsoids are displayed with 20% probability.

## **Section S3** Powder X-Ray Diffraction Patterns

**MOF-180**

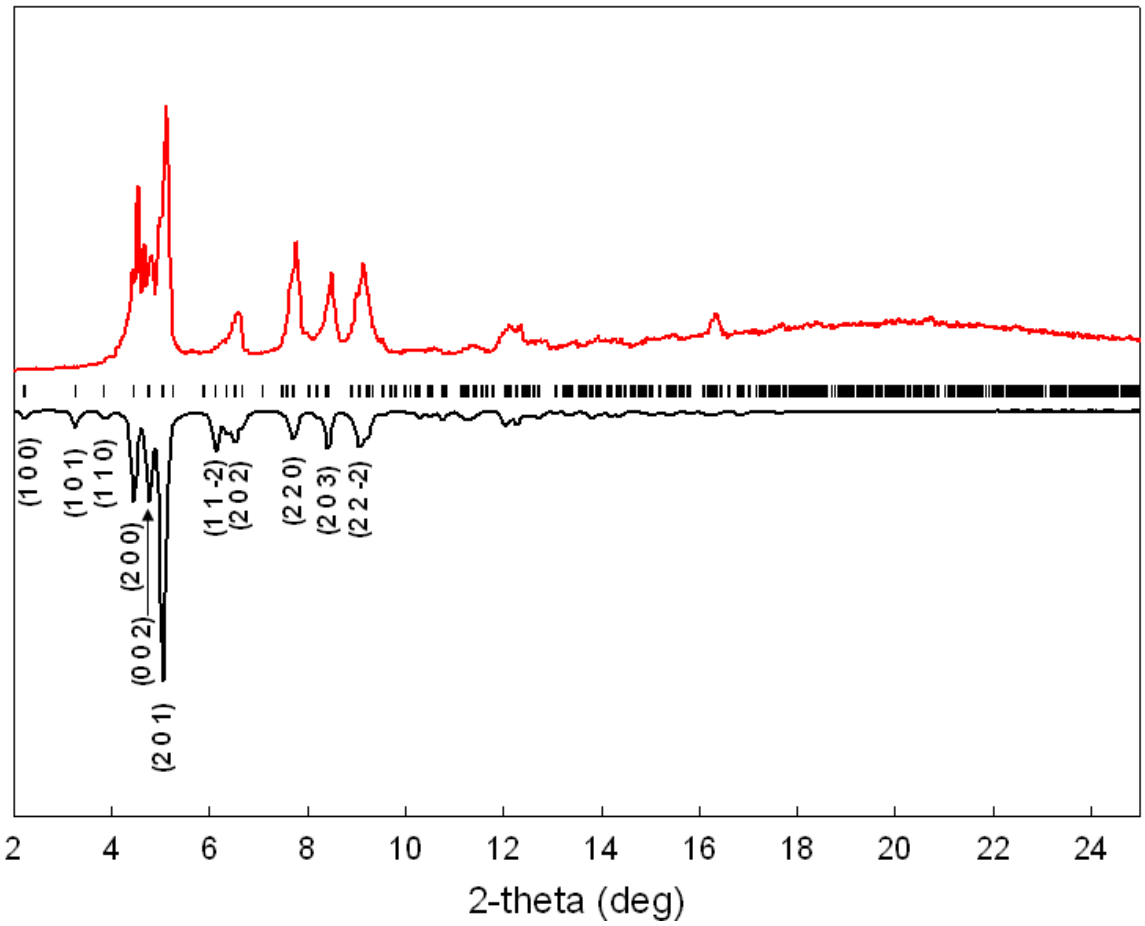


**Fig. S7.** Comparison of the experimental PXRD patterns of MOF-180: (Top) MOF-180 as-prepared (red), and simulated pattern (black) from a modeling structure.

**MOF-200**

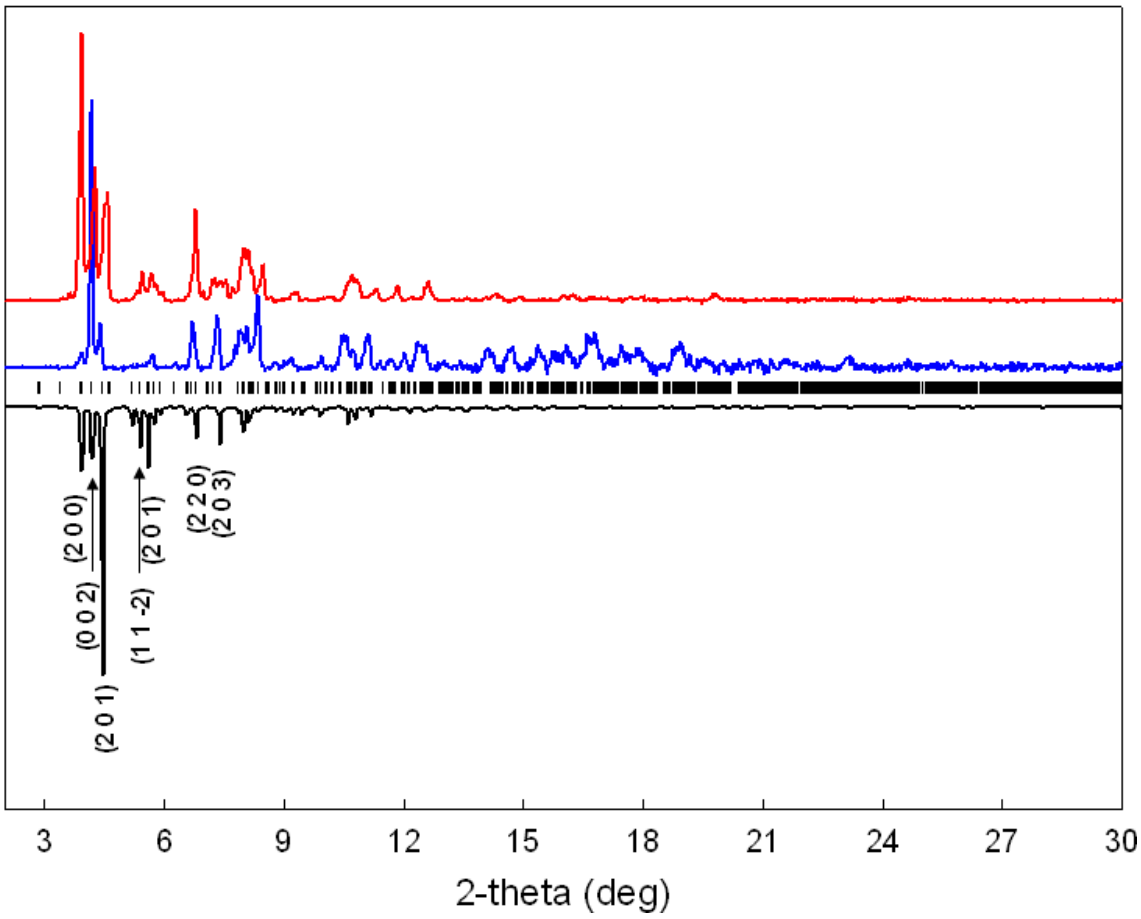


**Fig. S8.** Comparison of the experimental PXRD patterns of MOF-200: as-prepared (blue), evacuated after activated (red), and simulated pattern (black) from single-crystal X-ray data.

**MOF-205**

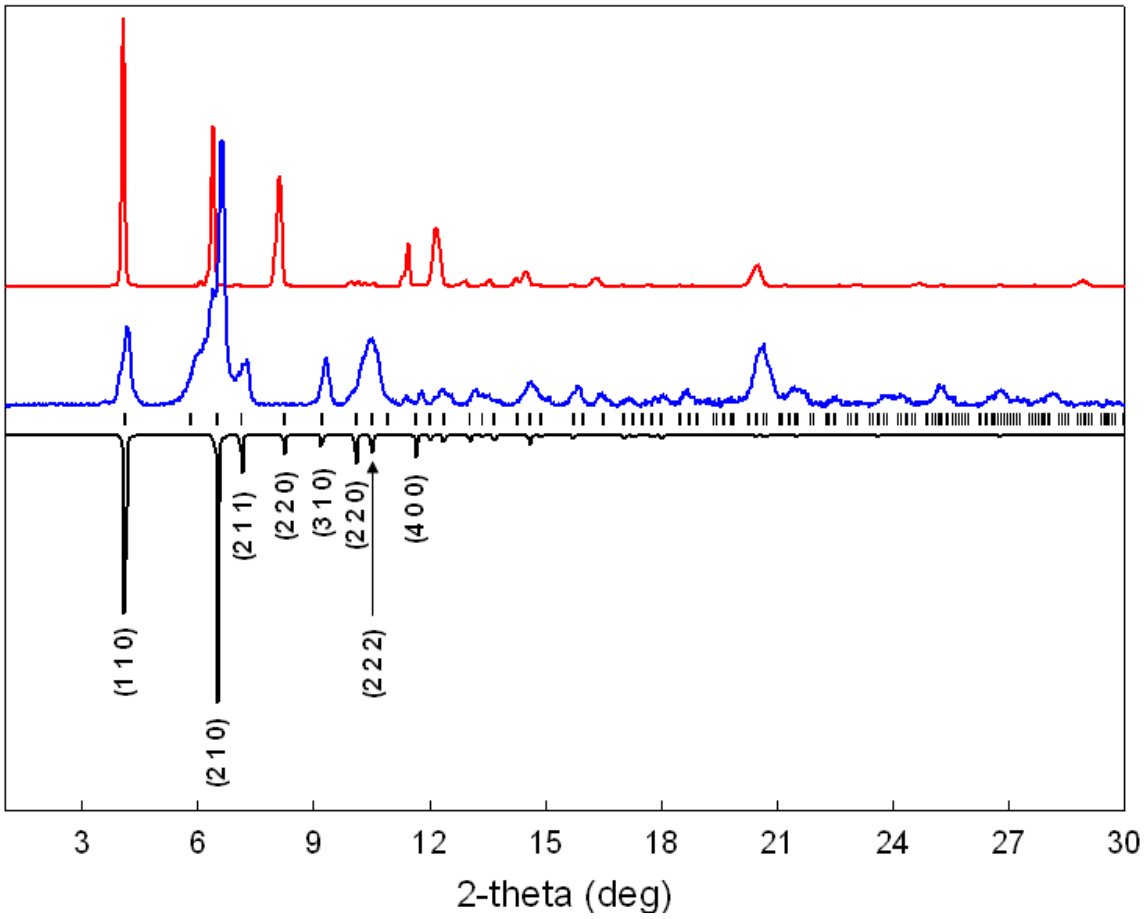


**Fig. S9.** Comparison of the XRD patterns of MOF-205; as-prepared (blue), activated (red) and simulated (black) from single-crystal X-ray data.

**MOF-210**

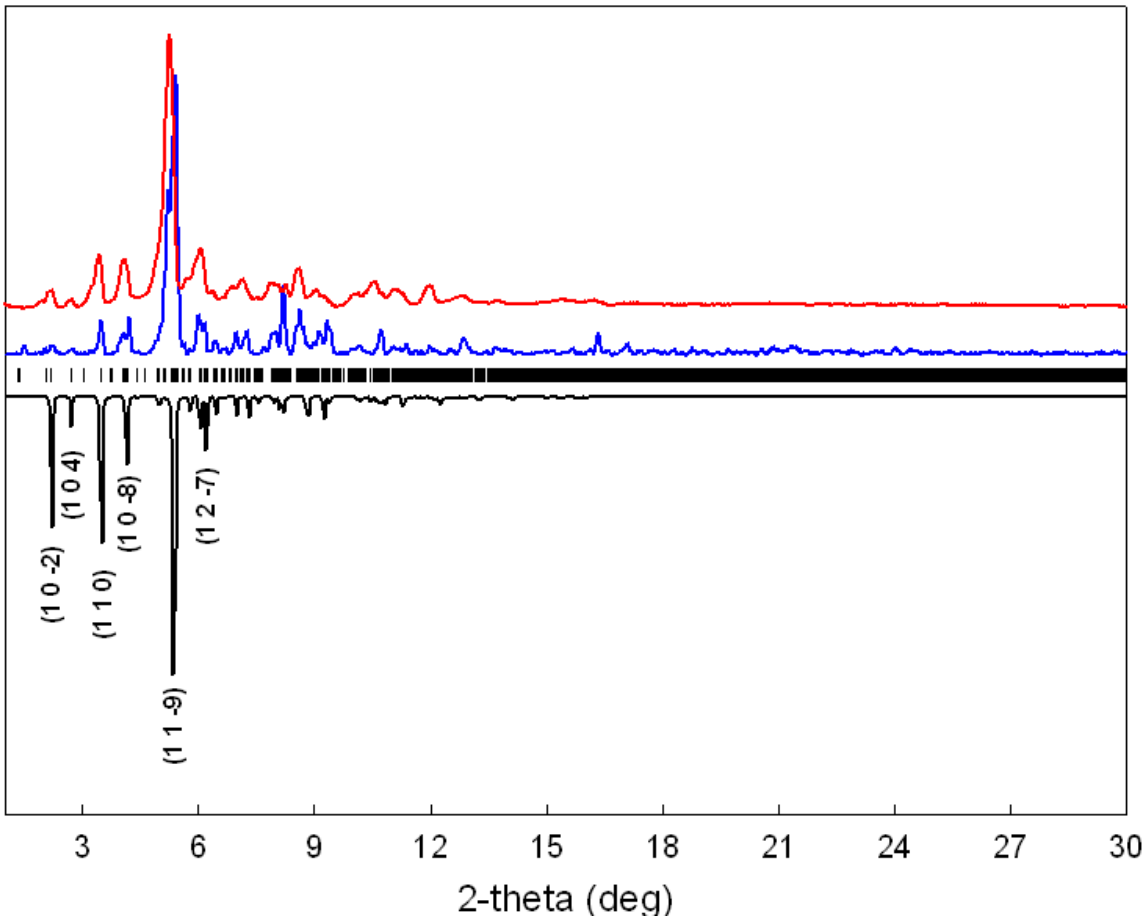


**Fig. S10.** Comparison of the XRD patterns of MOF-210; as-prepared (blue), activated (red) and simulated (black) from single-crystal X-ray data.

## **Section S4** $^{1}$H-NMR Analyses of Digested MOFs

As very porous MOFs lose the occluded solvents very quickly, elemental analysis usually can hardly give reliable information on the crystal formula. Thermogravimetric analysis (TGA) is generally not sensitive to discriminate chemical species. Therefore, $^{1}$H-NMR spectra for digested MOF crystals in DCl/DMSO were obtained on a Bruker 400 MHz NMR spectrometer for the estimation on the crystal composition. When a guest-occluded sample is dissolved in NMR solvents, the signals corresponding to both organic linkers and occluded solvent molecules should be observed, while guest-free crystals would produce only the signals of organic links. Based on the peak integration, the number of solvent molecules in the pore could be estimated, which was useful to suggest the crystal formula. For MOF-205 and -210, the ligand ratio could also be confirmed by the NMR measurements.

**MOF-180**

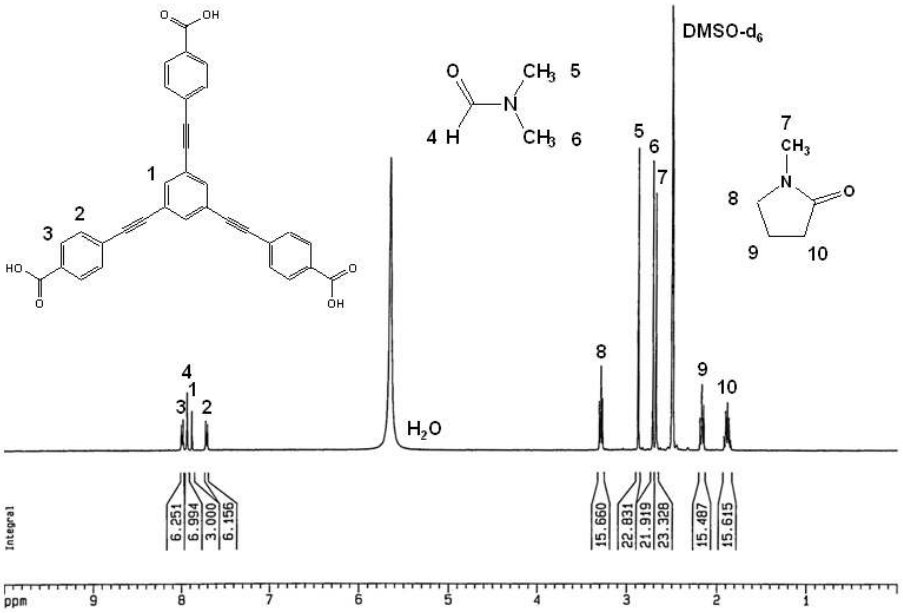


**Fig. S11.** $^{1}$H-NMR spectrum for as-prepared MOF-180 after digesting in DCl/DMSO-$d_6$ solution. The integration value of 26.8 at peaks **1** to **3** is attributed to 15 aromatic protons of $H_3$BTE. Comparing to the integration of BTE, 7.4 DMF (peaks **4** to **6**, 51.7 H) and 7.8 NMP (peaks **7** to **10**, 70.1 H) were also observed. From the molar ratio, the empirical formula has been estimated to be $Zn_4O(BTE)_2\cdot(DMF)_{14.8}(NMP)_{15.6}$.

**MOF-200**

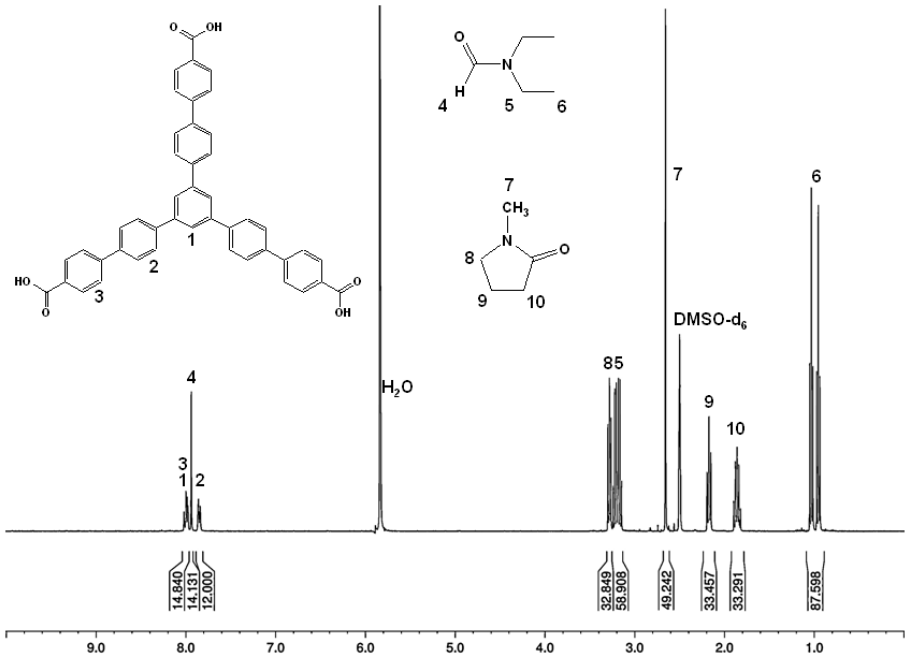


**Fig. S12.** $^{1}$H-NMR spectrum for as-prepared MOF-200 after digesting in DCl/DMSO-$d_6$ solution. The integration value of 26.8 at peaks **1** to **3** is attributed to 27 aromatic protons of $H_3BBC$. Comparing to the integration of BBC, 14.7 DEF (peaks **4** to **6**, 160.6 H) and 16.6 NMP (peaks **7** to **10**, 148.8 H) were also observed. From the molar ratio, the empirical formula has been estimated to be $Zn_4O(BBC)_2(H_2O)_3\cdot(DEF)_{29.4}(NMP)_{33.2}$.

**MOF-205**

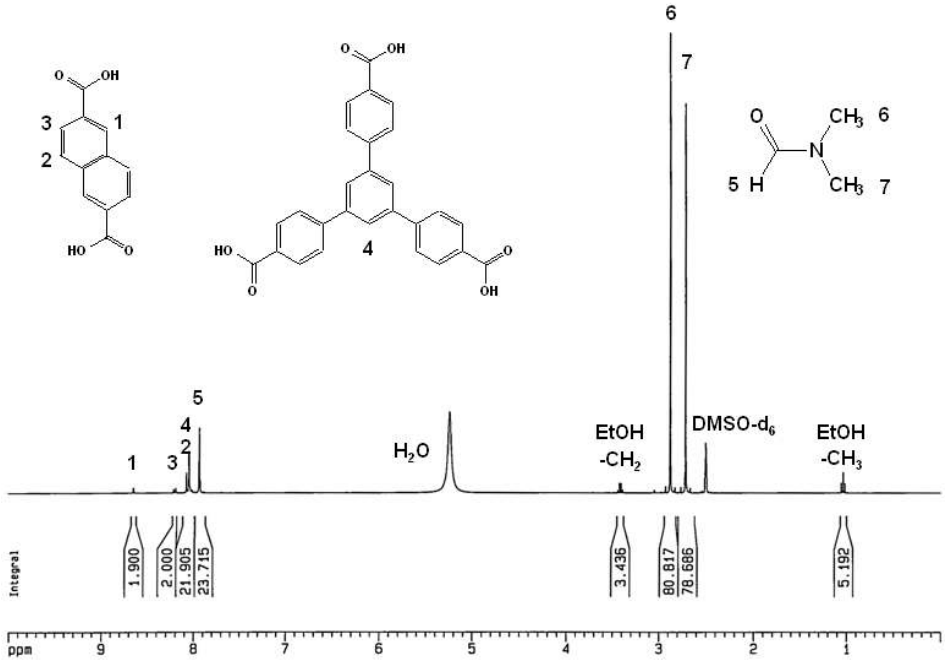


**Fig. S13.** $^{1}$H-NMR spectrum for as-prepared MOF-205 after digesting in DCl/DMSO-$d_6$ solution. The integration value of 25.8 at peaks **1** to **4** is attributed to 26 aromatic protons, which corresponds to 20 and 6 H of 4/3 $H_3$BTB and 1 $H_2$NDC, respectively. Comparing to the integration of BTB/NDC, 26.4 DMF (peaks **5** to **7**, 183.3 H) and 1.7 EtOH (8.69 H) were also observed. From the molar ratio, the empirical formula has been estimated to be $Zn_4O(BTB)_{4/3}(NDC)\cdot(DMF)_{26.4}(EtOH)_{1.7}$.

**MOF-205**

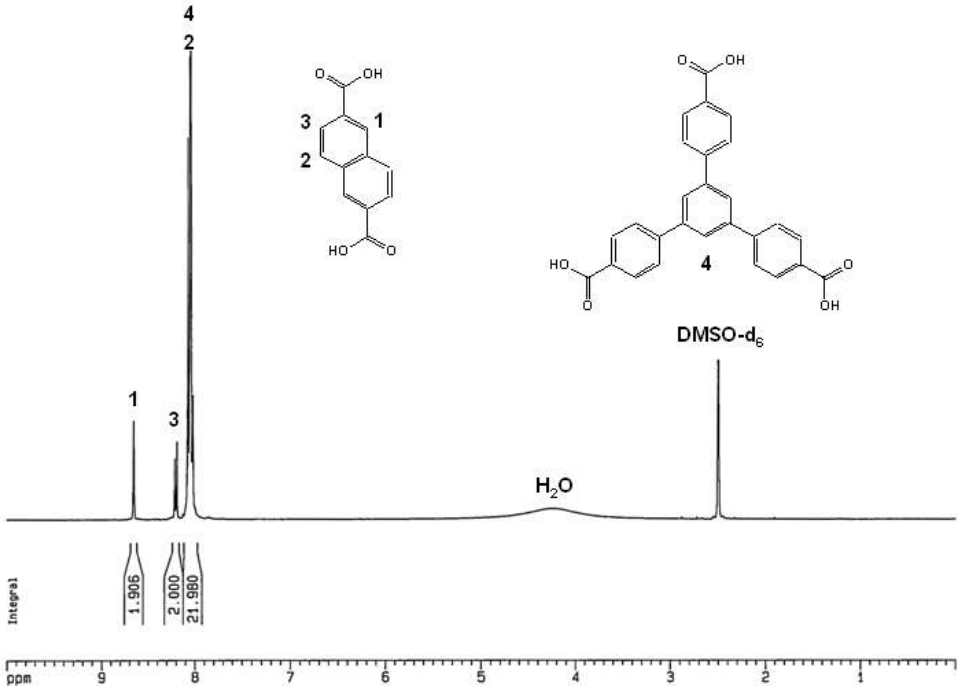


**Fig. S14.** $^{1}$H-NMR spectrum for guest-free MOF-205 after digesting in DCl/DMSO-$d_6$ solution. From the integration of peaks **1** and **3** (3.906 H), integration for $H_3BTB$ (peak **4**, aromatic proton only) is estimated to be 19.98 when the integration of peak **2** is 2 H. Based on the ratio of the integration of the peaks (19.98:5.906 = 4/3 BTB:NDC), the empirical formula has been estimated to be $Zn_4O(BTB)_{4/3}(NDC)$.

**MOF-210**

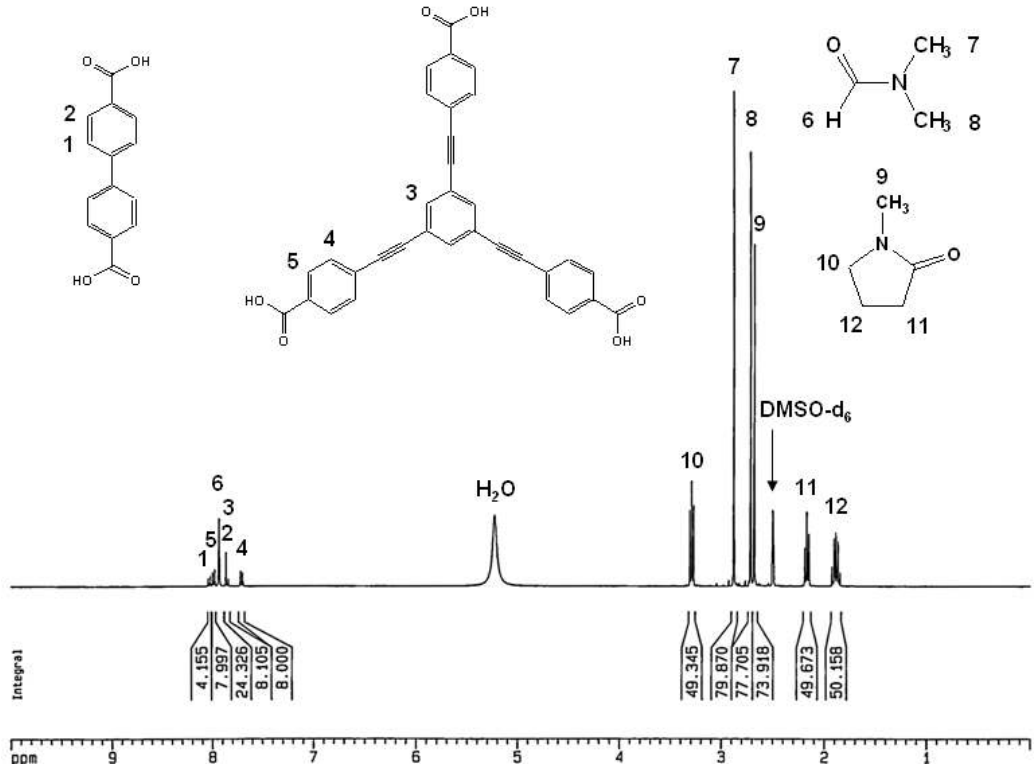


**Fig. S15.** $^{1}$H-NMR spectrum for as-prepared MOF-210 after digesting in DCl/DMSO-$d_6$ solution. The integration value 28.3 at peaks **1** to **5** is attributed to 28 aromatic protons, which corresponds to 20 and 8 H of 4/3 $H_3$BTE and 1 $H_2$BPDC, respectively. Comparing to the integration of BTE/NDC, 25.7 DMF (peaks **6** to **8**, 180 H) and 24.6 NMP (peaks **9** to **11**, 221 H) were also observed. From the molar ratio, the empirical formula has been estimated to be $Zn_4O(BTE)_{4/3}(BPDC)\cdot(DMF)_{25.7}(NMP)_{24.6}$.

**MOF-210**

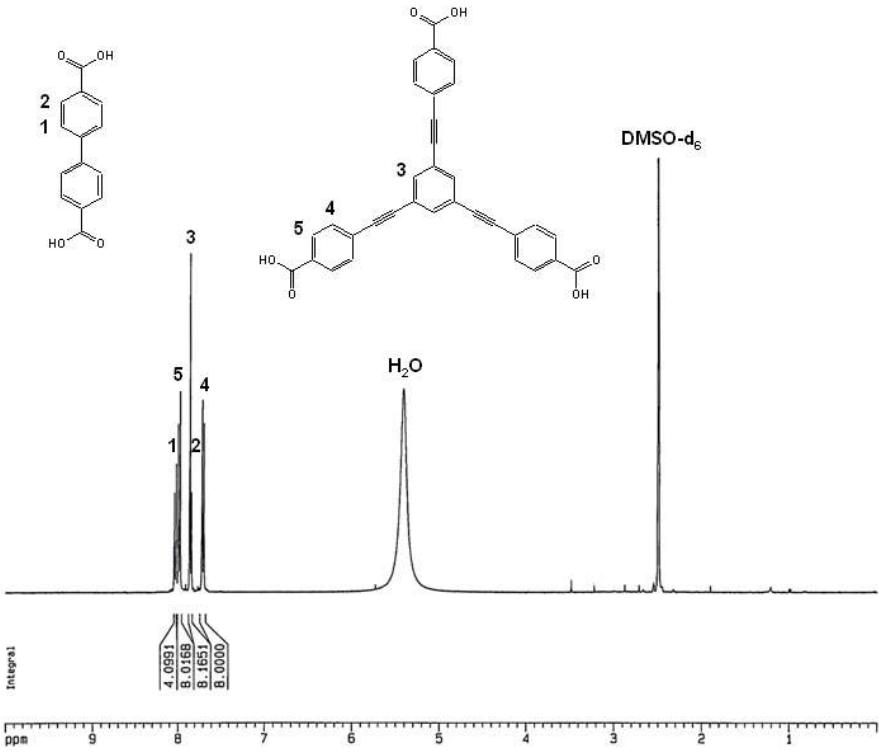


**Fig. S16.** $^{1}$H-NMR spectrum for guest-free MOF-210 after digesting in DCl/DMSO-$d_6$ solution. Based on the ratio of the integration of the peaks (20.1:8.2 = 4/3 BTE:BPDC), the empirical formula has been estimated to be $Zn_4O(BTE)_{4/3}(BPDC)$.

## **Section S5** Thermal Gravimetric Analyses

MOF-180 and 200 samples were heated at a constant rate of 5 °C $min^{-1}$ up to 700 °C on a TA Instruments Q-500 series thermal gravimetric analyzer in ambient atmosphere. MOF-205 and 210 samples were heated at a constant rate of 5 °C $min^{-1}$ up to 700 °C in ambient atmosphere on a Scinco TGA-S1000 apparatus. When the samples contain guest molecules, two distinguishable weight losses were observed before the final plateau. The first large decrease in weight % is due to the evaporation of occluded guest molecules. The weight loss probably due to the framework destruction was observed at between 300 to 500 °C. In the case of mixed link MOFs, there were small shoulder traces in the TGA curve because of the difference in the decomposition temperature of the links. The estimation on the guest contents based on the TAG analysis was in good agreement with the results obtained by the $^{1}$H-NMR experiments.

**MOF-180**

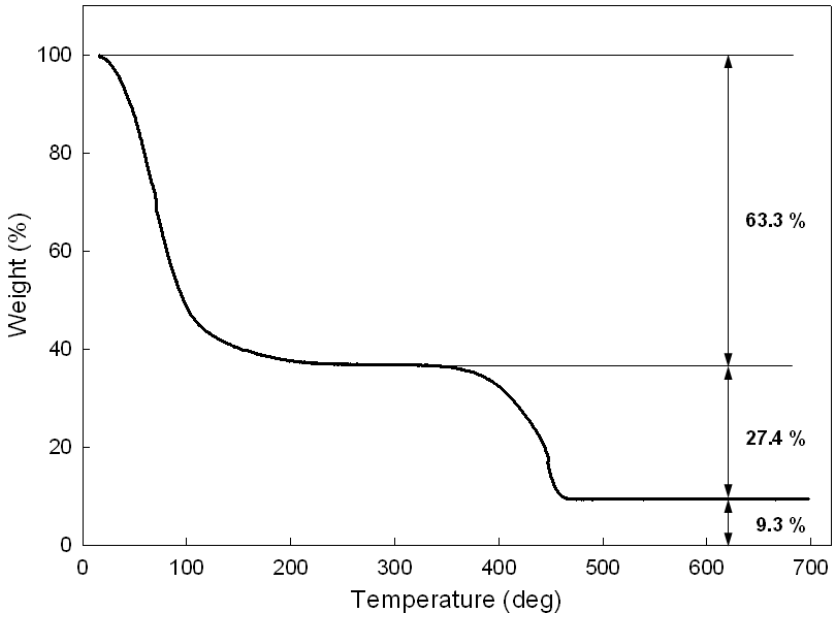


**Fig. S17.** TGA trace for as-prepared MOF-180.

**MOF-200**

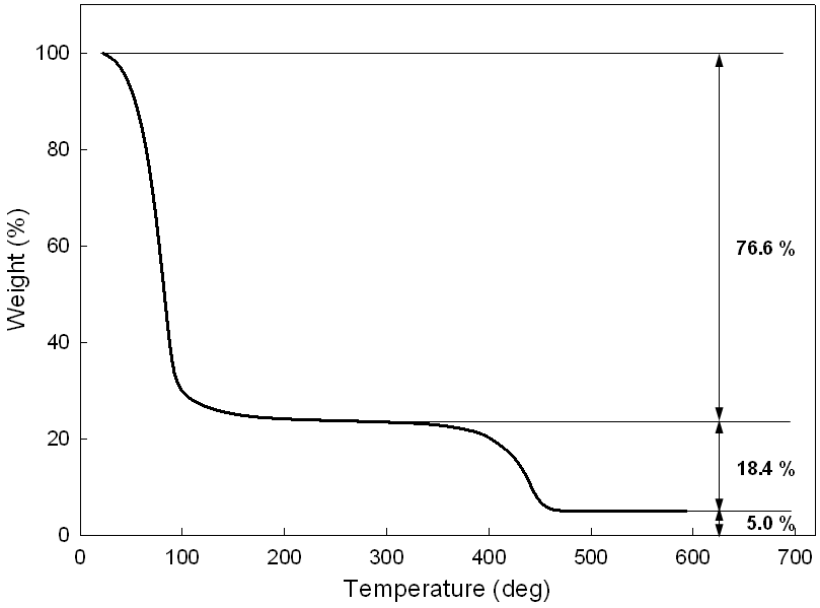


**Fig. S18.** TGA trace for as-prepared MOF-200.

**MOF-205**

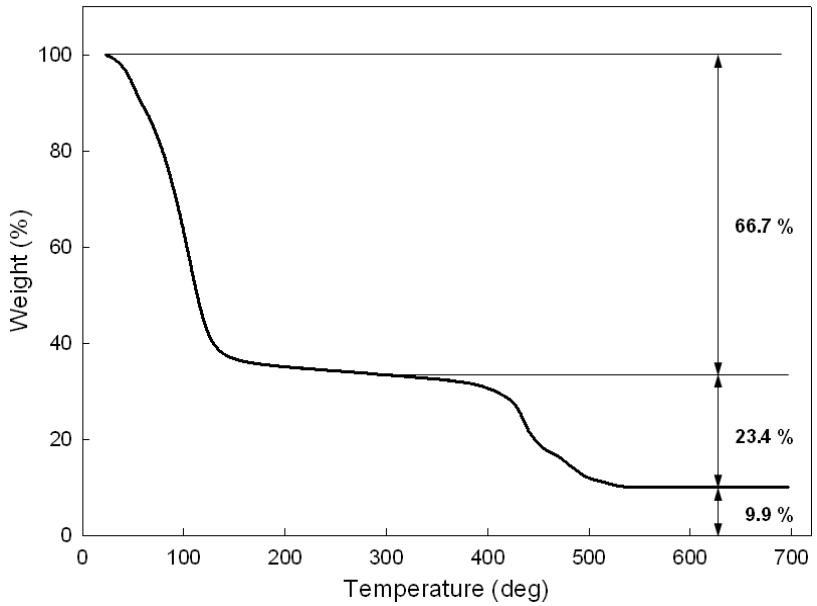


**Fig. S19.** TGA trace for as-prepared MOF-205.

**MOF-210**

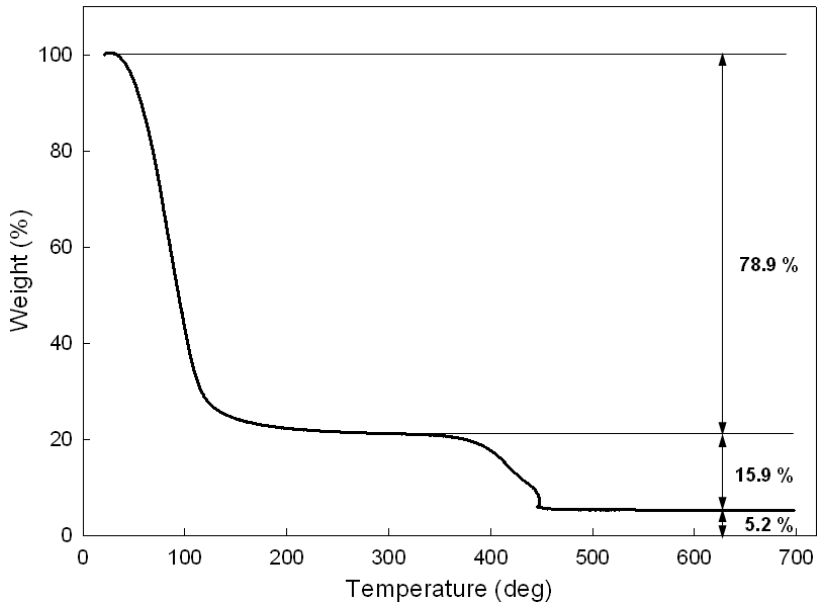


**Fig. S20.** TGA trace for as-prepared MOF-210.

# **Section S6** Grand Canonical Monte Carlo Simulations & Geometric Area Calculations

Atomistic grand canonical Monte Carlo (GCMC) simulations were performed to obtain nitrogen isotherms in MOF-200 and MOF-210. Prior to GCMC simulations we did density functional theory (DFT) calculations for each MOF to derive partial charges of the MOF atoms which are needed to calculate the electrostatic interaction energy between atoms during the GCMC simulations.

**DFT calculations**

DFT calculations were performed on clusters isolated from the unit cells of MOF-200 and MOF-210, with the atomic coordinates taken from the experimental crystallographic data. These clusters included building units (e.g. metal-oxide corner and the linker) representative of their respective unit cells. Details of structure and atom types on MOF-200 and MOF-210 clusters are shown in Figs. S21 and S22, respectively. All DFT calculations were performed with the Gaussian 03 (*S20*) software using the PBEPBE level of theory and the 6-31G* basis set, and partial atomic charges were extracted using the ChelpG (*S21*) method by fitting them to reproduce the electrostatic potential generated by the DFT calculations. Resulting partial charges for MOF-200 and MOF-210 are given in Tables S5 and S6, respectively.

**Grand canonical Monte Carlo (GCMC) simulations**

***Interaction potential***

The interaction energy between the atoms was computed through the Lennard-Jones (LJ) and Coulomb potentials

$$V_{ij} = 4\varepsilon_{ij}\left[\left(\frac{\sigma_{ij}}{r_{ij}}\right)^{12} - \left(\frac{\sigma_{ij}}{r_{ij}}\right)^{6}\right] + \frac{q_i q_j}{4\varepsilon_0 r_{ij}}$$

where $i$ and $j$ are interacting atoms, and $r_{ij}$ is the distance between atoms $i$ and $j$. $\varepsilon_{ij}$ and $\sigma_{ij}$ are the LJ well depth and diameter, respectively. $q_i$ and $q_j$ are the partial charges of the

interacting atoms, and $\varepsilon_0$ is the dielectric constant. LJ parameters between different types of sites were calculated using the Lorentz-Berthelot mixing rules.

***MOF models***

LJ parameters for MOF-200 and MOF-210 atoms were taken from the DREIDING (*S22*) force field. Partial charges for MOF atoms were derived from DFT calculations as explained above. Table S7 shows the LJ parameters for all atom types found in MOF-200 and MOF-210.

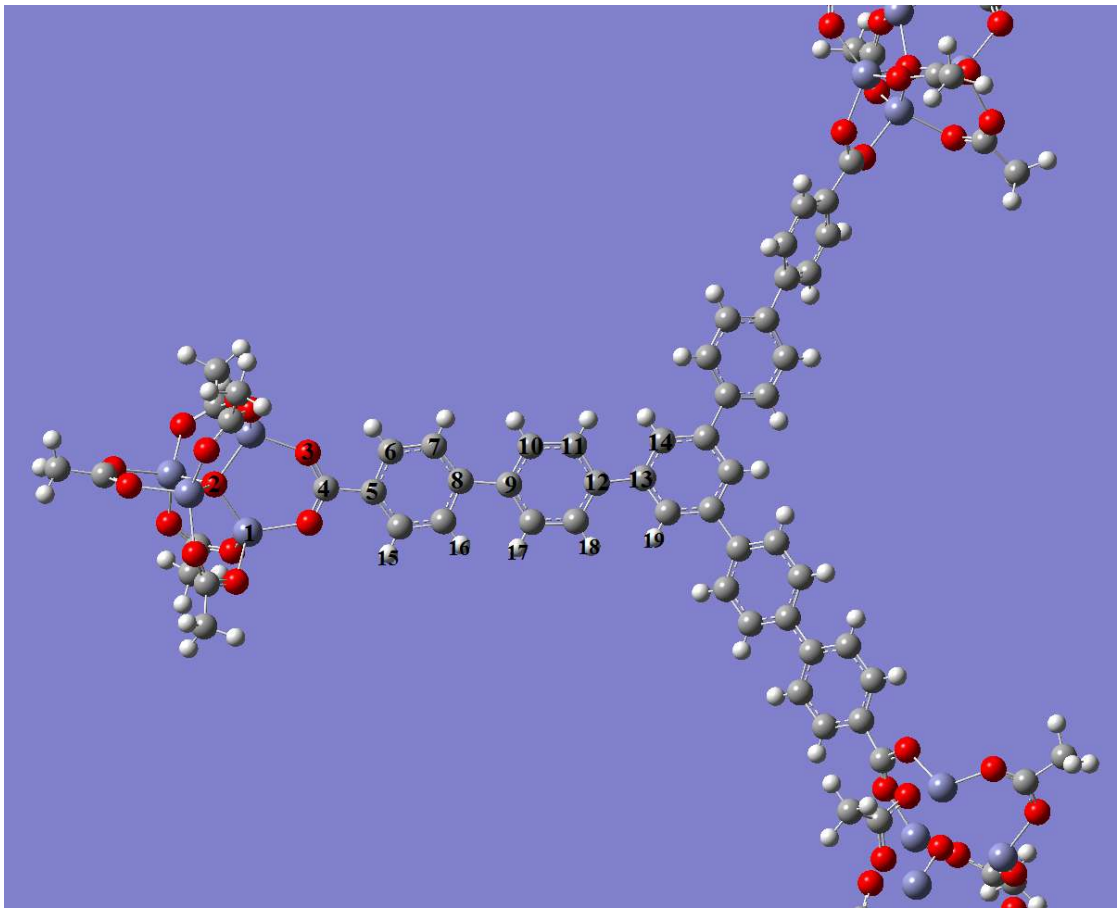


**Fig. S21.** Cluster used for deriving partial charges on MOF-200 atoms.

**Table S5.** Partial atomic charges for MOF-200 atoms.

| Atom No | 1 | 2 | 3 | 4 | 5 | 6 |
|---|---|---|---|---|---|---|
| Charge (e) | 1.225 (Zn) | -1.390 (O) | -0.603 (O) | 0.560 (C) | 0.076 (C) | -0.174 (C) |
| Atom No | 7 | 8 | 9 | 10 | 11 | 12 |
| Charge (e) | -0.154 (C) | 0.055 (C) | 0.036 (C) | -0.143 (C) | -0.167 (C) | 0.067 (C) |
| Atom No | 13 | 14 | 15 | 16 | 17 | 18 |
| Charge (e) | 0.051 (C) | -0.196 (H) | 0.150 (H) | 0.138 (H) | 0.132 (H) | 0.136 (H) |
| Atom No | 19 | | | | | |
| Charge (e) | 0.136 (H) | | | | | |

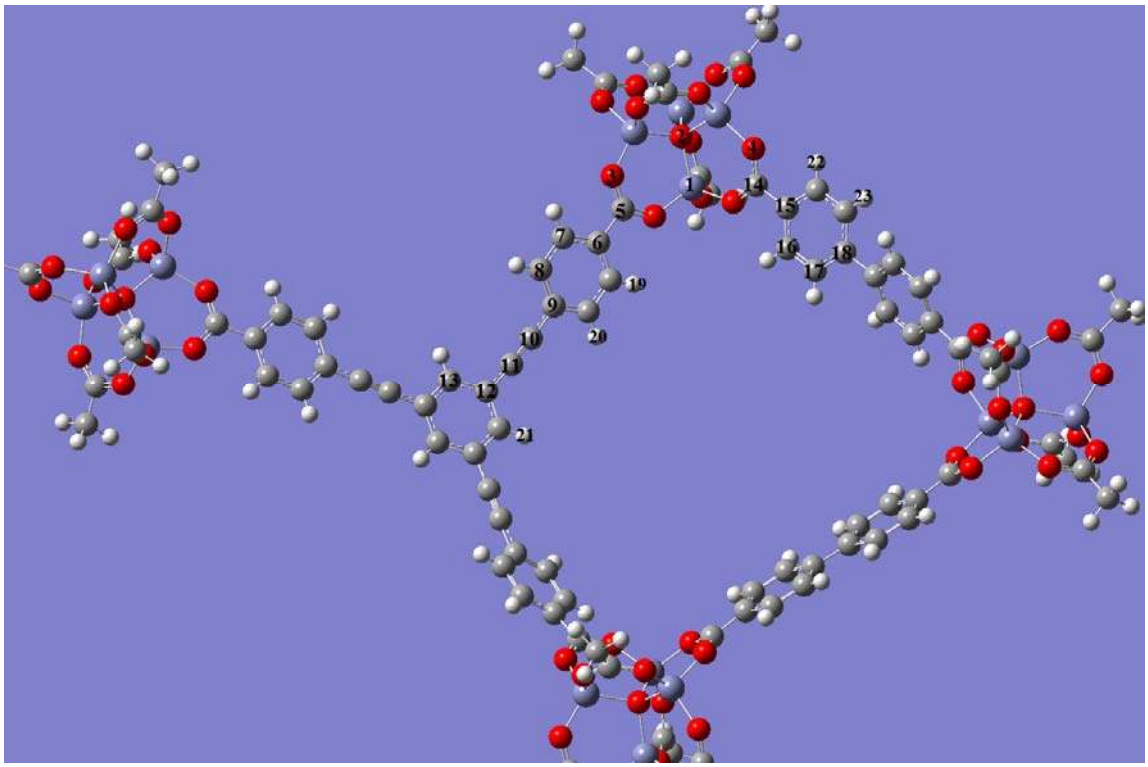

**Fig. S22.** Cluster used for deriving partial charges on MOF-210 atoms.

**Table S6.** Partial atomic charges for MOF-210 atoms.

| Atom No. | 1 | 2 | 3 | 4 | 5 | 6 |
|---|---|---|---|---|---|---|
| Charge (e) | 1.406 (Zn) | -1.592 (O) | -0.679 (O) | -0.679 (O) | 0.622 (C) | 0.046 (C) |
| Atom No. | 7 | 8 | 9 | 10 | 11 | 12 |
| Charge (e) | -0.159 (C) | -0.166 (C) | 0.194 (C) | -0.136 (C) | -0.115 (C) | 0.195 (C) |
| Atom No. | 13 | 14 | 15 | 16 | 17 | 18 |
| Charge (e) | -0.254 (C) | 0.625 (C) | 0.027 (C) | -0.135 (C) | -0.162 (C) | 0.060 (C) |
| Atom No. | 19 | 20 | 21 | 22 | 23 | |
| Charge (e) | 0.154 (H) | 0.150 (H) | 0.178 (H) | 0.143 (H) | 0.139 (H) | |

**Table S7.** LJ parameters for MOF-200 and MOF-210 atoms.

| Atom type | σ (Å) | $\varepsilon/k_B$ (K) |
|---|---|---|
| C | 3.473 | 47.856 |
| O | 3.033 | 48.158 |
| H | 2.846 | 7.649 |
| Zn | 4.045 | 27.677 |

***Nitrogen Model***

Nitrogen molecule was modeled using the TraPPE (*S23*) force field. This force field was originally fit to reproduce the vapor-liquid coexistence curve of nitrogen. In this force field nitrogen molecule is a rigid structure where the N-N bond length is fixed at its experimental value of 1.10 Å. This model also reproduces the experimental gas-phase quadrupole moment of nitrogen by placing partial charges on N atoms and on a point located at the center of mass (COM) of the nitrogen molecule. Table S8 shows the LJ parameters and partial charges for nitrogen.

**Table S8.** LJ parameters and partial charges for the sites in the nitrogen molecule.

| | σ (Å) | $\varepsilon/k_B$ (K) | q (e) |
|---|---|---|---|
| N | 3.31 | 36.0 | -0.482 |
| $N_2$ COM | 0 | 0 | 0.964 |

***General GCMC simulation settings***

All GCMC simulations included a 10000 cycle equilibration period followed by a 10000 cycle production run. A cycle consists of *n* Monte Carlo steps; where *n* is equal to the number of molecules (which fluctuates during a GCMC simulation). All simulations included random insertion/deletion, translation and rotation moves of nitrogen molecules with equal probabilities. MOF atoms were held fixed at their crystallographic positions. An LJ cutoff distance of 12.5 Å was used for all simulations. The Ewald sum technique was used to compute the electrostatic interactions. One unit cell of MOF-200 or MOF-210 (Rhombohedral representation) was used for the simulations. Nitrogen isotherms were simulated at 77 K up to 0.9 bar. Fugacities needed to run the GCMC simulations were calculated using the Peng-Robinson equation of state. All simulated adsorption data reported in this work are the excess quantities, as it is the proper quantity for comparison with experimental data as explained elsewhere (*S24*).

**Table S9.** Simulated surface areas and pore volume of MOFs.

| | BET SA / $m^2\ g^{-1}$ | Langmuir SA / $m^2\ g^{-1}$ | Pore volume / $cm^3\ g^{-1}$ |
|---|---|---|---|
| MOF-200 | 6260 | 12040 | 4.19 |
| MOF-210 | 6580 | 10450 | 3.63 |

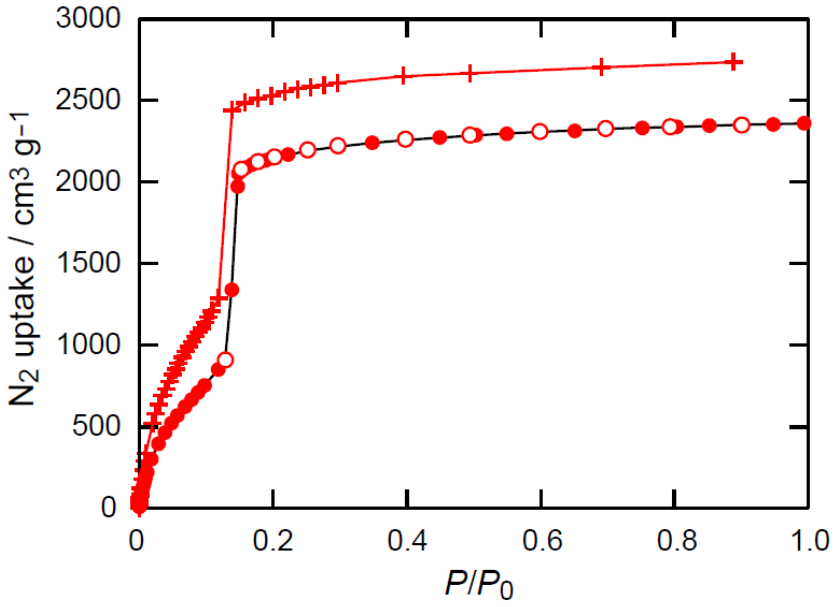


**Fig. S23.** Simulated $N_2$ isotherm for MOF-200 (+). Experimental data were overlaid (circles).

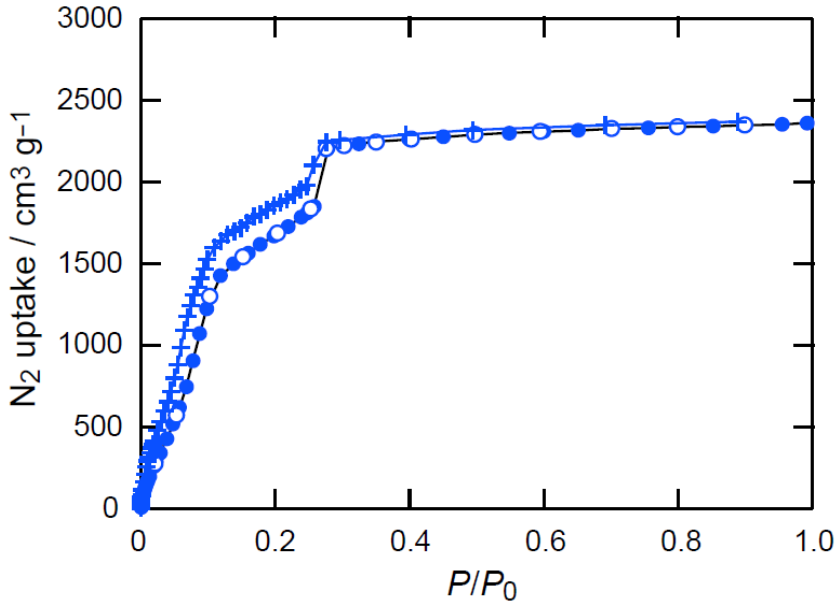


**Fig. S24.** Simulated $N_2$ isotherm for MOF-210 (+). Experimental data were overlaid (circles).

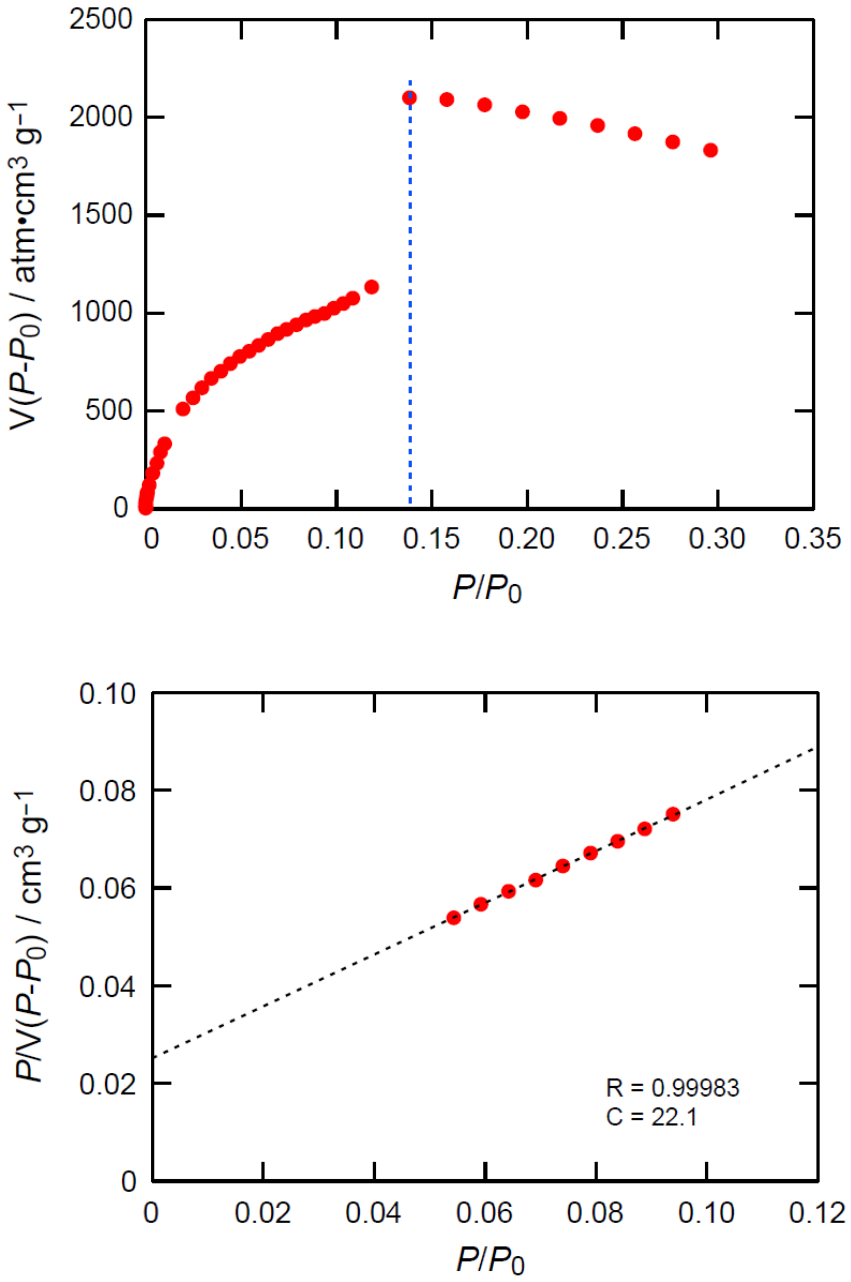


**Fig. S25.** (TOP) V($P_0$ - $P$) vs. $P/P_0$ for simulated MOF-200 isotherm. Only the range below $P/P_0$ = 0.14 satisfies the first consistency criterion for applying the BET theory (*S25*). (Bottom) Plot of the linear region for the BET equation.

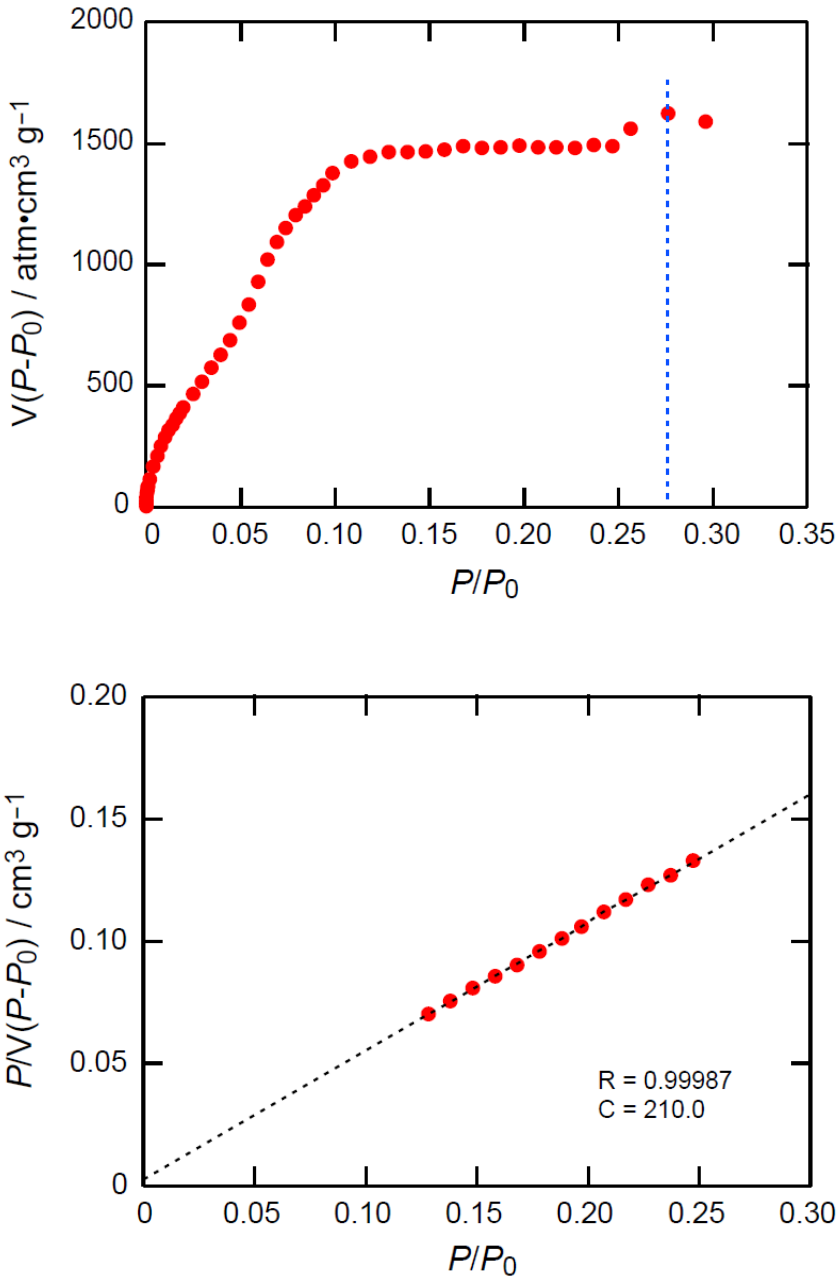


**Fig. S26.** (TOP) V($P_0$ - $P$) vs. $P/P_0$ for simulated MOF-210 isotherm. Only the range below $P/P_0$ = 0.27 satisfies the first consistency criterion for applying the BET theory (*S25*). (Bottom) Plot of the linear region for the BET equation.

***Geometric surface area calculations***

Geometric surface areas of the MOFs listed in Table 1 were calculated by rolling a sphere probe over the framework atoms as explained in the work of Düren *et al.* (*S26*). The probe diameter was equal to the van der Waals diameter of nitrogen, which is 3.72 Å (*S27*). The diameters of the framework atoms were also set to their van der Waals diameters (Table S10) which were calculated by multiplying their Lennard-Jones well-depth diameters, σ, by $2^{1/6}$. The σ values of all framework atoms were taken from the DREIDING force field (*S22*) except for the Cu and Cr atoms, which were taken from the Universal Force Field (UFF) (*S28*).

**Table S10.** Van der Waals diameters of the framework atoms of MOFs listed in Table 1.

| Atom type | van der Waals diameter (Å) |
|---|---|
| C | 3.898 |
| O | 3.404 |
| H | 3.195 |
| N | 3.663 |
| S | 4.030 |
| Zn | 4.540 |
| Cu | 3.495 |
| Cr | 3.023 |

## Section S7 Gas Adsorption Analyses

**Activation of MOFs.**

As-synthesized sample of MOF-205 were immersed in dichloromethane for 3 days; during the exchange the dichloromethane was refreshed three times. The resulting dichloromethane-exchanged sample of MOF-205 was transferred as a suspension to a quartz cell and the solvent was decanted. The wet sample was then evacuated ($10^{-3}$ Torr) at room temperature for 10 h then at 100 °C for 12 h.

As-synthesized samples of MOF-200 and 210 were immersed in DEF and dichloromethane for 3 days, respectively, during which the activation solvent was decanted and freshly replenished three times. Obtained samples were immersed in acetone for 12 h, during which the activation solvent was replenished more than five times. The sample was evacuated with supercritical $CO_2$ in a Tousimis Samdri PVT-3D critical point dryer (*S29*, *S30*). Briefly, the acetone-containing sample was placed in the chamber and acetone was completely exchanged with liquid $CO_2$. After that the chamber containing the sample and liquid $CO_2$ was heated up around 40 °C and kept under the supercritical condition (typically 1300 psi) for 1 h. The $CO_2$ was slowly vented (ca. 1 h) from the chamber at around 40 °C, yielding porous material.

**Low-pressure gas adsorption measurements.**

Low-pressure gas adsorption experiments (up to 760 torr) were carried out on a Quantachrome AUTOSORB-1 automatic volumetric instrument. Ultrahigh-purity-grade $N_2$ and He gases were used in all adsorption measurements. The $N_2$ (77 K) isotherms were measured using a liquid nitrogen bath (77 K).

**BET surface area of MOFs.**

A BET surface area was obtained by using the data points on the adsorption branch of the $N_2$ isotherm (see Section S5) (*S25*). The BET surface area for MOF-200, 205, and 210 were calculated to be 4530, 4460, and 6240 $m^2\ g^{-1}$, respectively.

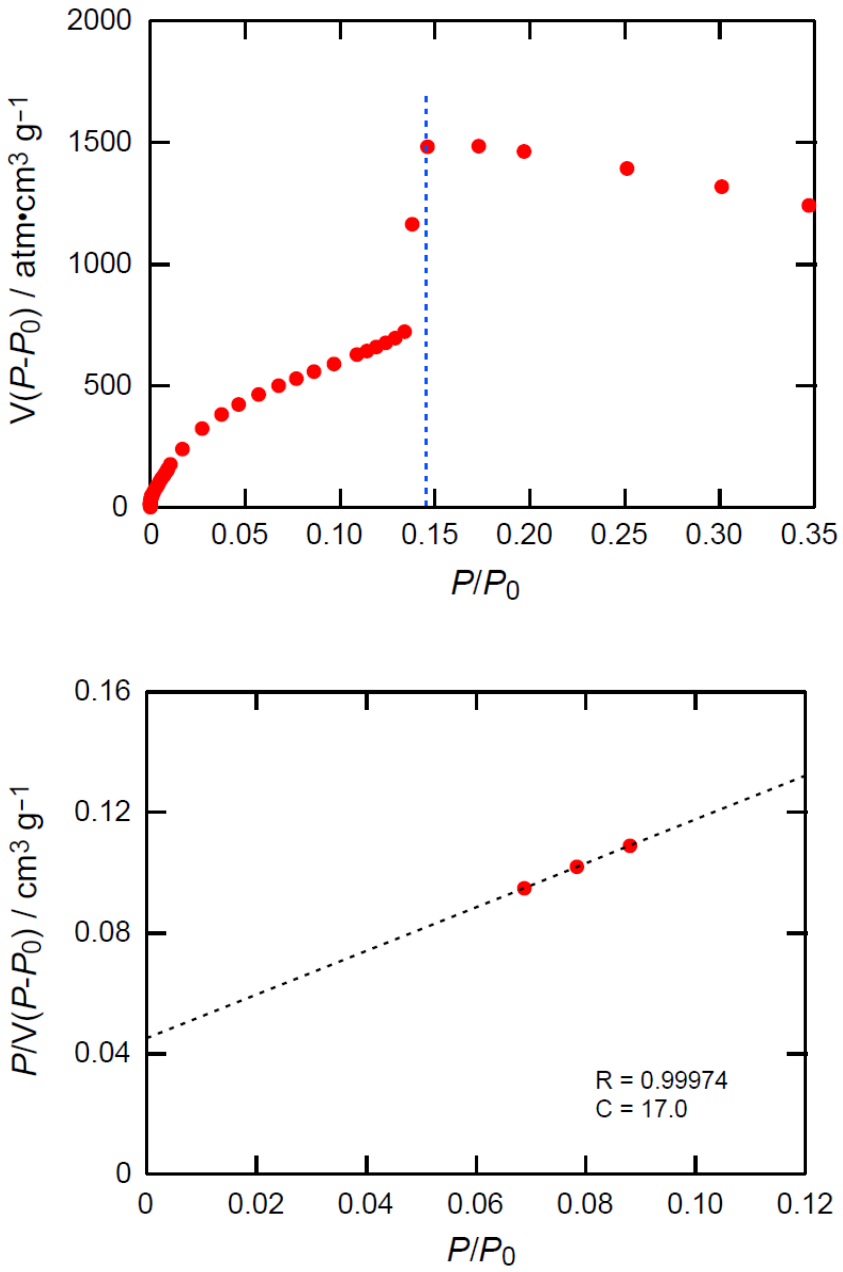


**Fig. S27.** (TOP) V($P_0$ - $P$) vs. $P/P_0$ for MOF-200. Only the range below $P/P_0$ = 0.14 satisfies the first consistency criterion for applying the BET theory. (Bottom) Plot of the linear region for the BET equation.

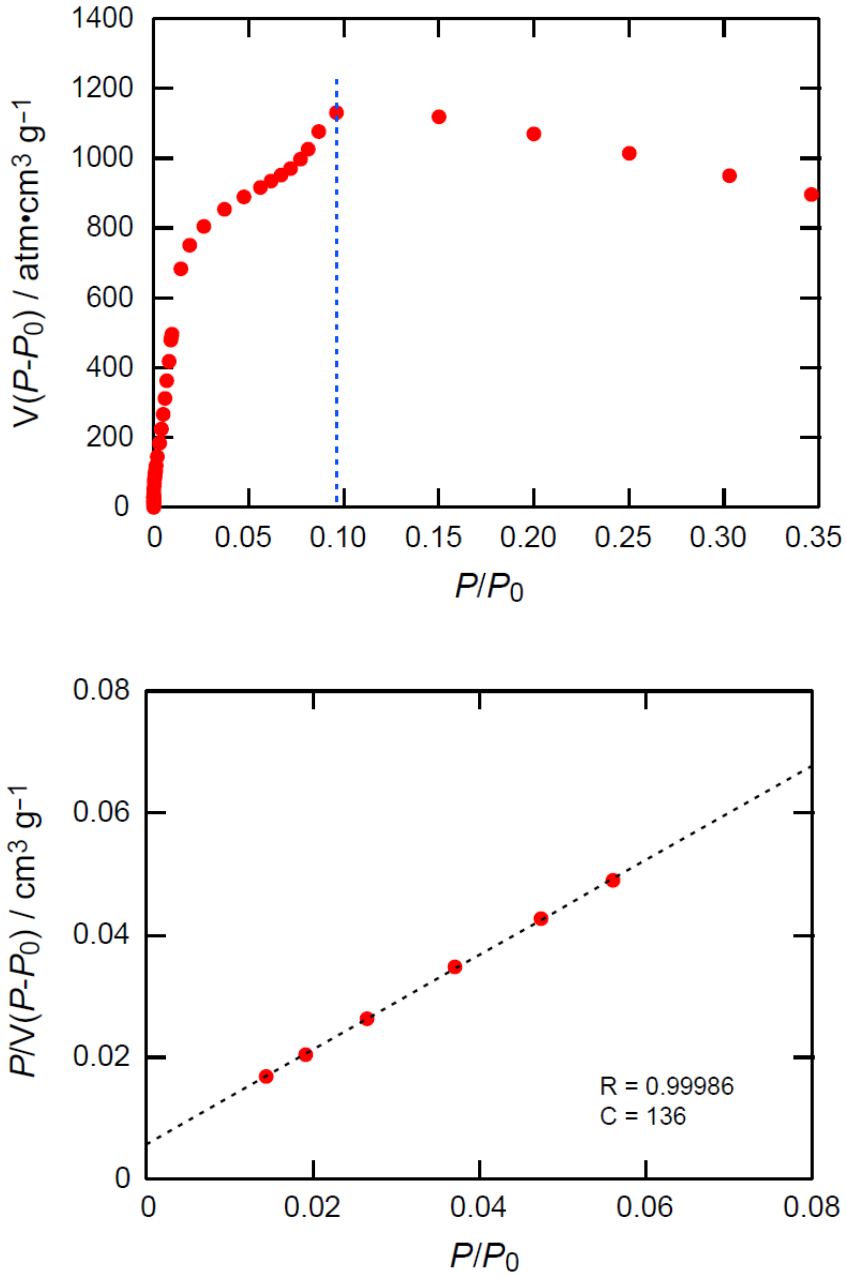


**Fig. S28.** (TOP) V($P_0$ - $P$) vs. $P/P_0$ for MOF-205. Only the range below $P/P_0$ = 0.09 satisfies the first consistency criterion for applying the BET theory. (Bottom) Plot of the linear region for the BET equation.

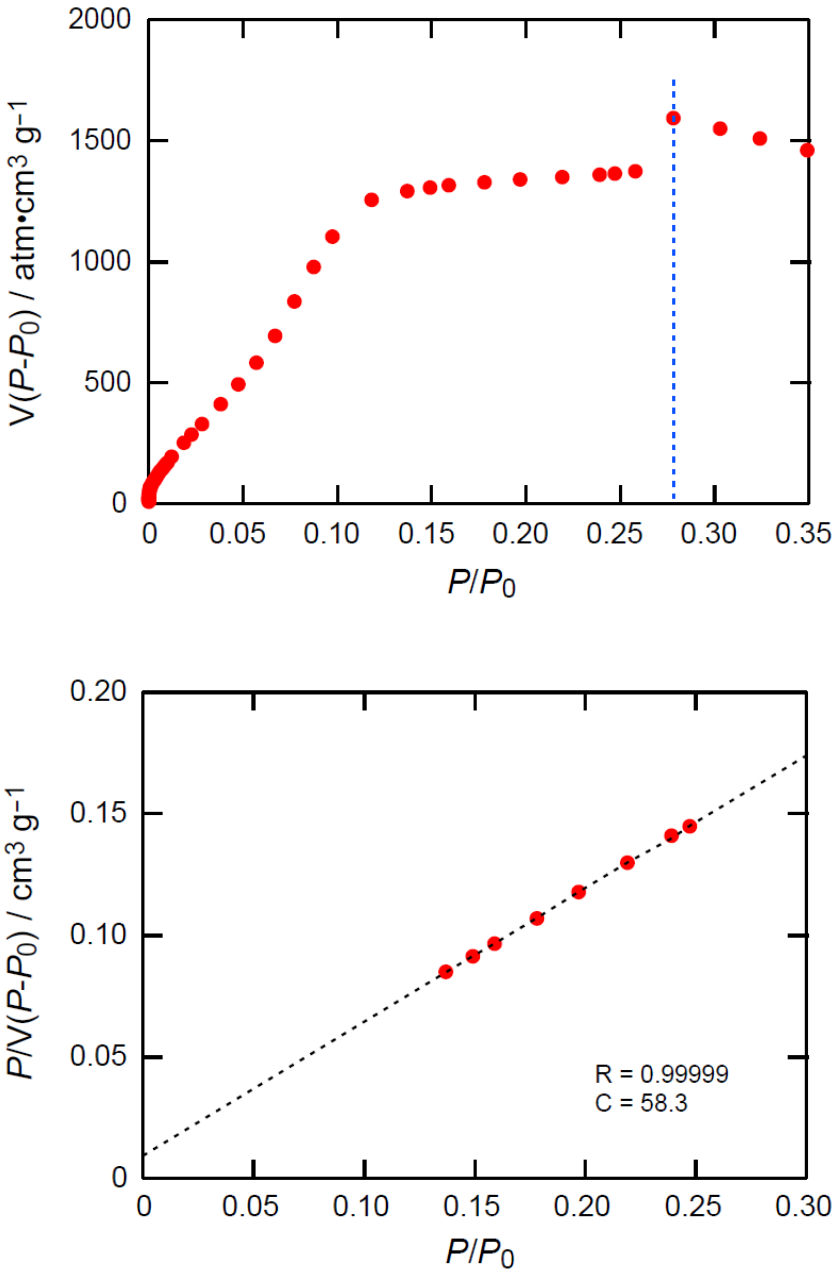


**Fig. S29.** (TOP) V($P_0$ - $P$) vs. $P/P_0$ for MOF-210. Only the range below $P/P_0$ = 0.27 satisfies the first consistency criterion for applying the BET theory. (Bottom) Plot of the linear region for the BET equation.

**Table S11.** Porosity data of highly porous MOFs. ND, no data.

| Compound | RCSR code | Linker | Void volume (%) | Crystal density (g cm$^{-3}$) | $A_{BET}$‡ (m$^2$ g$^{-1}$) | $A_{Lang}$‡ (m$^2$ g$^{-1}$) | $A_{geo}$‡,† (m$^2$ g$^{-1}$) | $V_p$‡ (cm$^3$ g$^{-1}$) | Reference |
|---|---|---|---|---|---|---|---|---|---|
| MOF-5 | **pcu** | BDC | 79 | 0.59 | 2860<br>3800¶ | 3480<br>4400¶ | 3390 | 1.22<br>1.55¶ | This work |
| MOF-177 | **qom** | BTB | 83 | 0.43 | 4500 | 5340 | 4740 | 1.89 | (*S31*) |
| MOF-180 | **qom** | BTE | 89 | 0.25 | ND | ND | 6080 | ND | This work |
| MOF-200 | **qom** | BBC | 90 | 0.22 | 4530 | 10400 | 6400 | 3.59 | This work |
| MOF-205 | **ith-d** | BTB,NDC | 85 | 0.38 | 4460 | 6170 | 4680 | 2.16 | This work |
| MOF-210 | **toz** | BTE,BPDC | 89 | 0.25 | 6240 | 10400 | 5850 | 3.60 | This work |
| UMCM-2 | **umt** | BTB,T2DC‡ | 83 | 0.40 | 5200 | 6060 | 4360 | 2.32 | (*S32*) |
| NOTT-112 | **ntt** | TDBB‡ | 80 | 0.48 | 3800 | ND | 3950 | 1.67 | (*S33*) |
| PCN-14 | **nbo** | ADIP‡ | 66 | 0.83 | 1750 | 2180 | 1860 | 0.87 | (*S34*) |
| MIL-101c | **mtn-e** | BDC | 83 | 0.44 | 4230 | 5900 | 2880 | 2.15 | (*S35*, *S36*) |

‡Acronyms: $A_{BET}$, $A_{Lang}$, and $A_{geo}$ are the BET, Langmuir, and geometric surface areas; $V_p$ is the measured pore volume; $H_2$T2DC = thieno[3,2-*b*]thiophene-2,5-dicarboxylic acid, $H_6$TDBB = 1,3,5-tris(3′,5′-dicarboxy[1,1′-biphenyl]-4-yl-)benzene; $H_4$ADIP = 5,5′-(9,10-anthracenediyl)di-isophthalic acid. †See Section S6. ¶Values taken from Ref. S37.

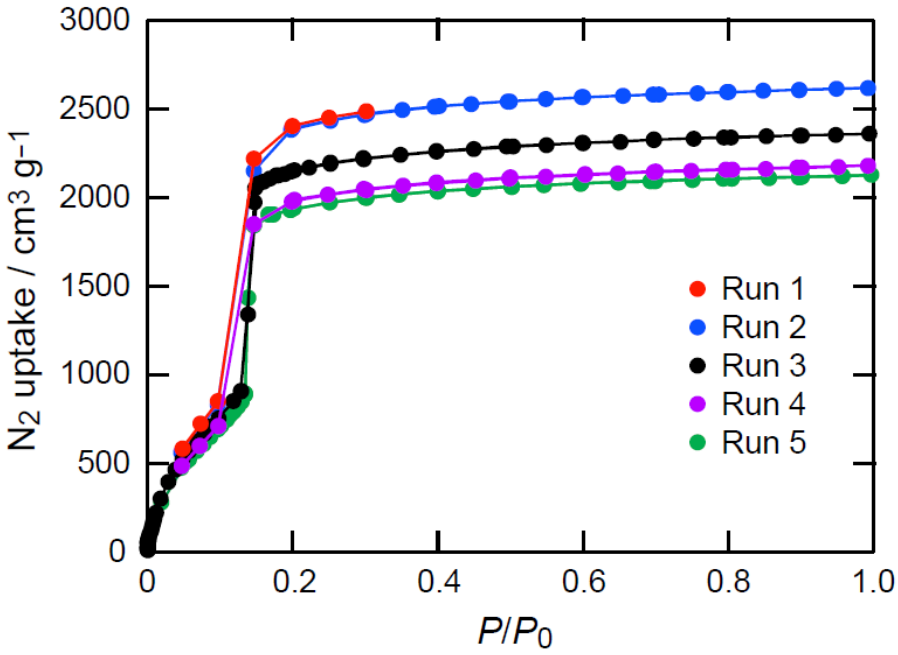


**Fig. S30.** $N_2$ isotherms of independently prepared MOF-200.

Fig. S30 demonstrates the $N_2$ isotherms of MOF-200. The sample for Run #3 (same as the isotherm in Fig. 3A) was prepared by a conventional method (small scale synthesis), while rest of them are prepared by the improved method. As shown here, $N_2$ uptakes are in the range of 2300 $cm^3\ g^{-1} \pm 230\ cm^3\ g^{-1}$ (i.e. within 10% error).

**High-pressure gas adsorption measurements.**

High-pressure gas adsorption isotherms for MOF-205 were gravimetrically recorded on a GHP-300 gravimetric high-pressure analyzer from VTI Corporation (currently TA Instruments) (*S31*). To obtain the excess adsorption isotherm, all data points were corrected for buoyancy and the thermal gradient that arises between the balance and the sample bucket. For MOF-200 and 210 equilibrium gas adsorption isotherms were measured using the static volumetric method in an HPA-100 from the VTI Corporation (currently Particulate Systems). Ultra-high-purity grade $H_2$, $CH_4$, He (99.999% purity), and $CO_2$ gases (99.995% purity) were used throughout the high-pressure adsorption experiments. When $H_2$ gas was used, water and other condensable impurities were removed with a liquid nitrogen trap. Detailed experimental procedures for gravimetric and volumetric measurements were published in Ref. S31.

**Estimation of total gas uptake.**

Although the surface excess mass is a useful concept, from the viewpoint of gas storage, the total amount that a material can store is more relevant. However, at high temperatures and pressures (i.e., above the critical point of gases), the density profile of the adsorbed phase becomes more diffused and, therefore, it is not possible to distinguish between the adsorbed and bulk phases with the present techniques. In this situation the surface excess is the only experimentally accessible quantity, and there is not a reliable method to estimate the absolute adsorbed amount with high accuracy, although many efforts have been devoted to resolve this issue. Therefore, we estimate the absolute amount of hydrogen adsorbed using a simple equation: (total uptake) = (excess uptake) + (bulk density of gas) × (pore volume).

Needless to say, the volumetric gas uptake (e.g., g $L^{-1}$ unit) is also influenced by the packing factor of the crystalline materials. The packing density is influenced by both shape and size of the materials and usually is below unity, although these numbers for MOFs are not available here. Indeed, the volumetric uptake should be 10-25% smaller compared to the data in Table S12, if the packing density is 0.7.

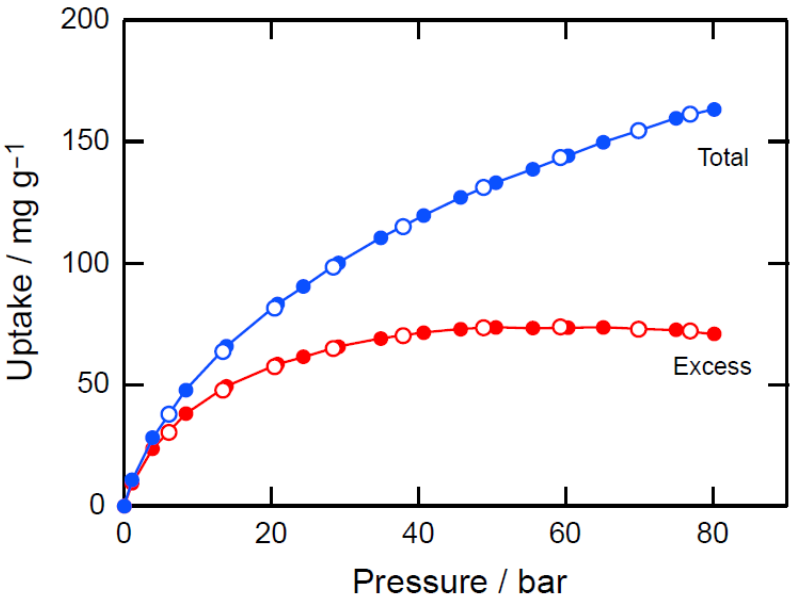


**Fig. S31.** High-pressure $H_2$ isotherms for MOF-200 measured at 77 K. Red and blue symbols represent surface excess and total uptakes, and filled and open symbols represent adsorption and desorption branches. Connecting traces are guides for eyes.

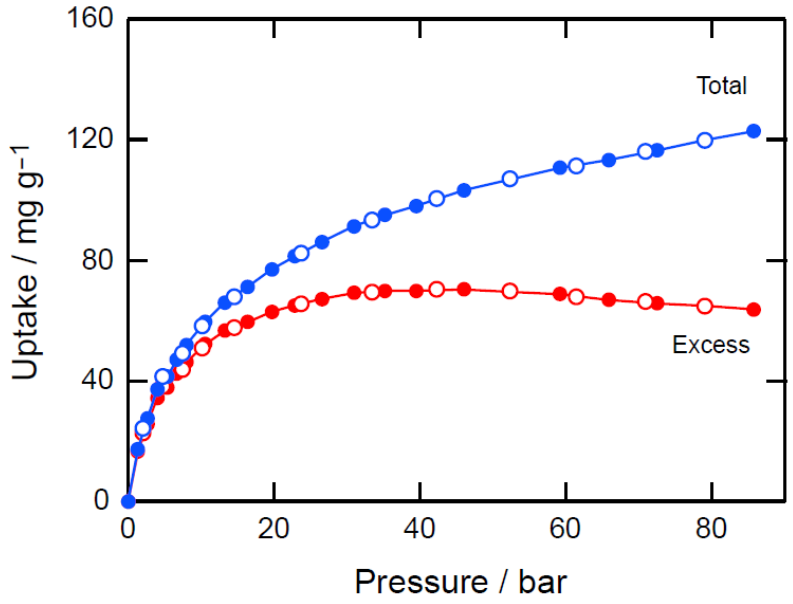


**Fig. S32.** High-pressure $H_2$ isotherms for MOF-205 measured at 77 K. All symbols are the same as in Fig. S31.

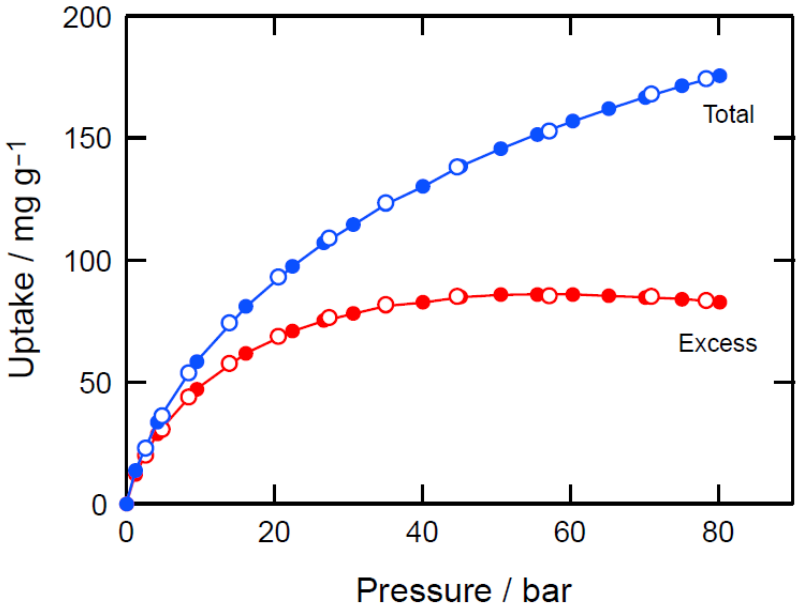


**Fig. S33.** High-pressure $H_2$ isotherms for MOF-210 measured at 77 K. All symbols are the same as in Fig. S31.

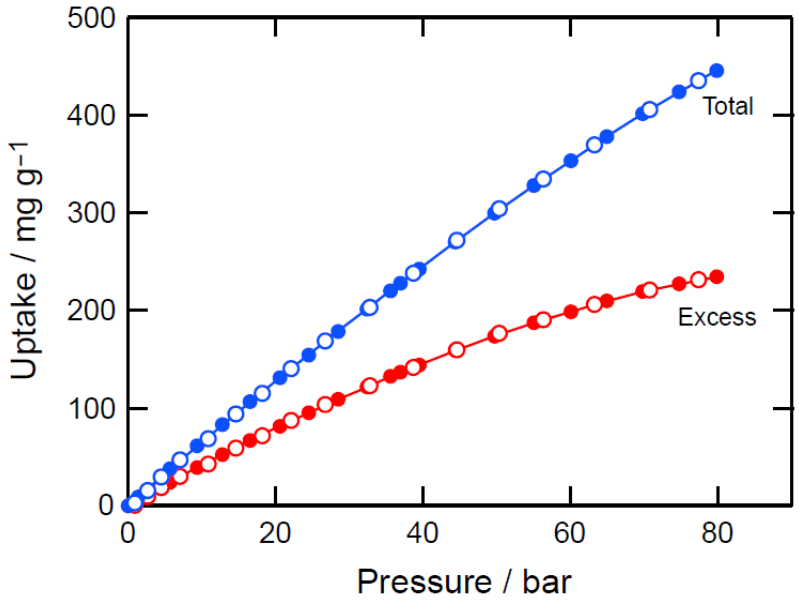


**Fig. S34.** High-pressure $CH_4$ isotherms for MOF-200 measured at 298 K. All symbols are the same as in Fig. S31.

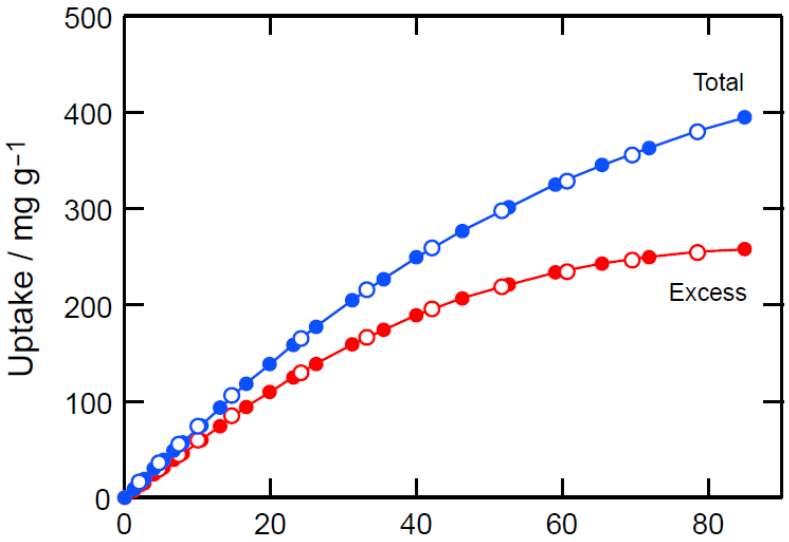


**Fig. S35.** High-pressure $CH_4$ isotherms for MOF-205 measured at 298 K. All symbols are the same as in Fig. S31.

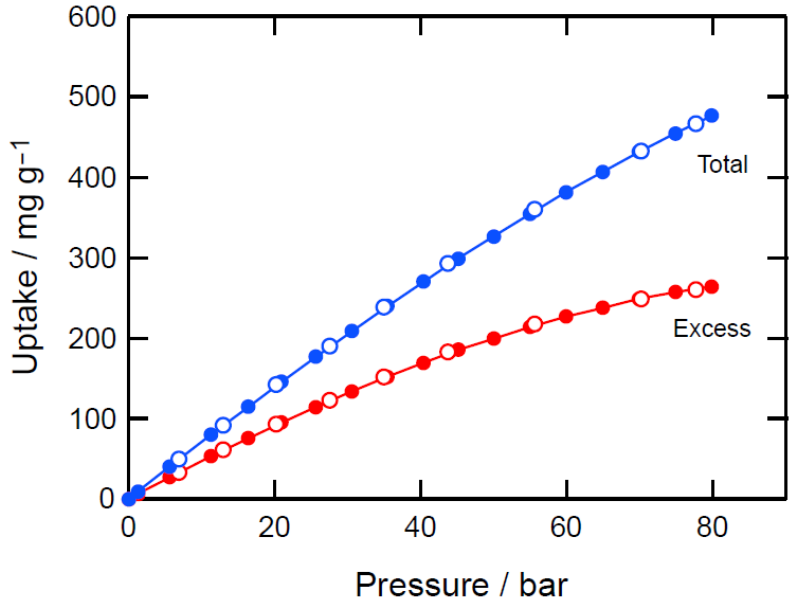


**Fig. S36.** High-pressure $CH_4$ isotherms for MOF-210 measured at 298 K. All symbols are the same as in Fig. S31.

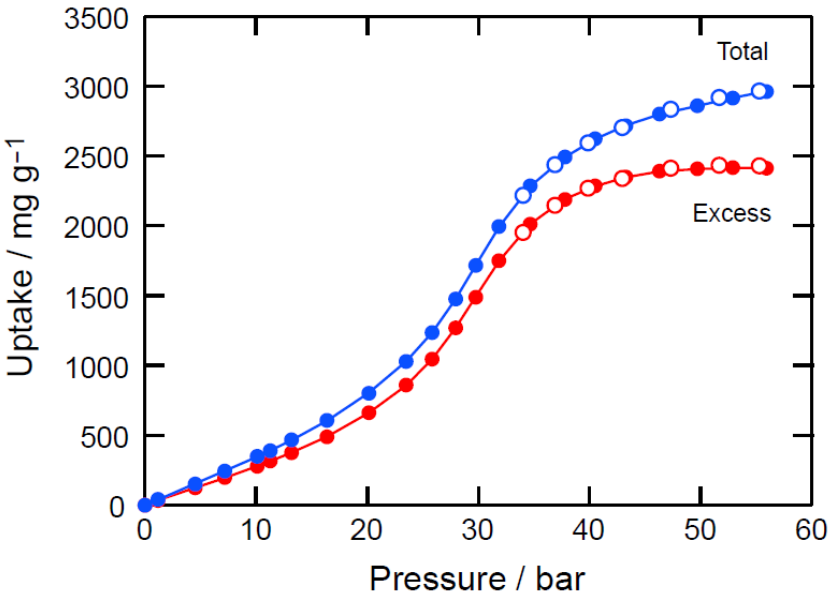


**Fig. S37.** High-pressure $CO_2$ isotherms for MOF-200 measured at 298 K. All symbols are the same as in Fig. S31.

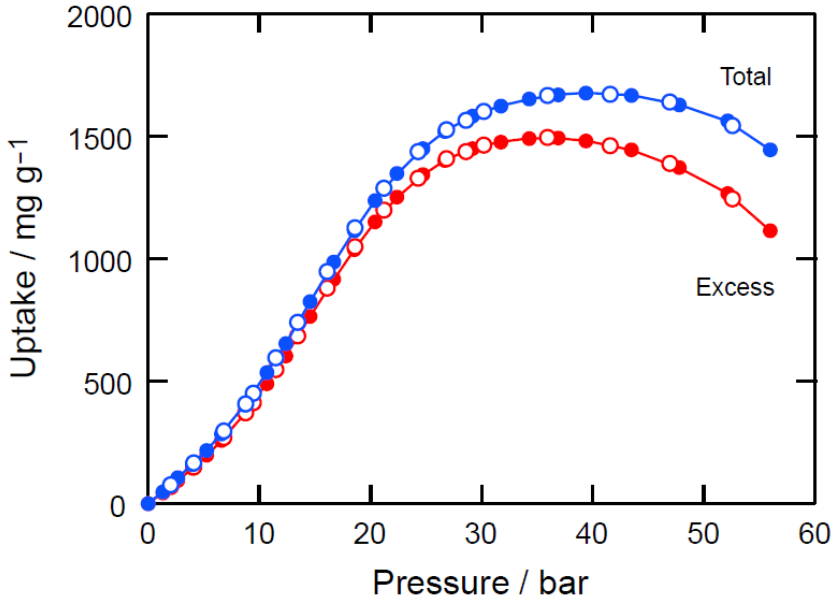


**Fig. S38.** High-pressure $CO_2$ isotherms for MOF-205 measured at 298 K. All symbols are the same as in Fig. S31.

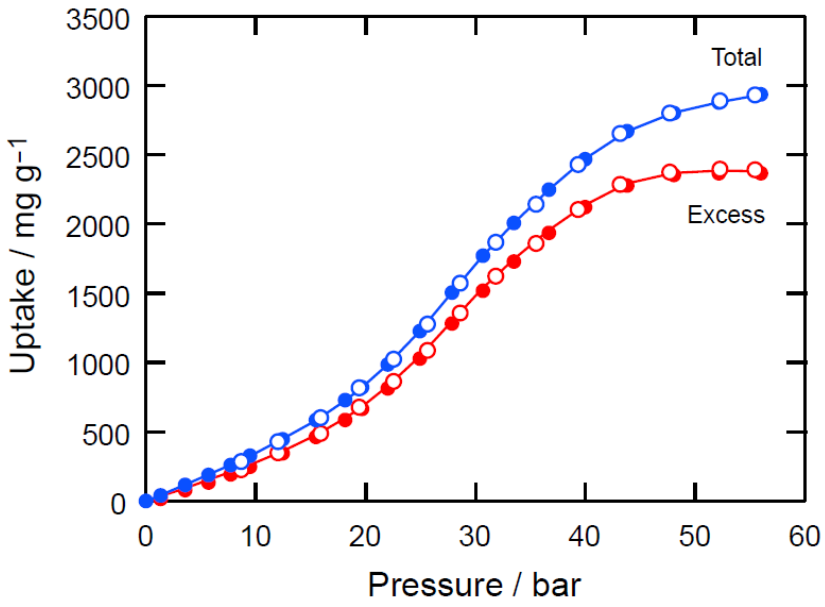


**Fig. S39.** High-pressure $CO_2$ isotherms for MOF-210 measured at 298 K. All symbols are the same as in Fig. S31.

**Table S12.** Summary of high-pressure adsorption measurements for MOFs. ND, no data; NA, not applicable.

| Compound | $H_2$ at 77 K and 80 bar | | | $CH_4$ at 298 K and 80 bar | | | $CO_2$ at 298 K and 50 bar | | | Reference |
|---|---|---|---|---|---|---|---|---|---|---|
| | Excess[‡] ($mg\ g^{-1}$) | **Total ($mg\ g^{-1}$)** | Total[†] ($g\ L^{-1}$) | Excess ($mg\ g^{-1}$) | **Total ($mg\ g^{-1}$)** | Total[†] ($g\ L^{-1}$) | Excess[‡] ($mg\ g^{-1}$) | **Total ($mg\ g^{-1}$)** | Total[†] ($g\ L^{-1}$) | |
| MOF-5 | 53 | **82** | 48 | 165 | **250** | 148 | 864 | **1030** | 608 | This work |
| | 76 | **106** | 63 | ND | ND | ND | ND | ND | ND | (*S37*) |
| MOF-177 | 73 | **116** | 50 | 243 | **345** | 147 | 1356 | **1550** | 662 | (*S31*), this work |
| MOF-200 | 74 | **163** | 36 | 234 | **445** | 99 | 2437 | **2830** | 628 | This work |
| MOF-205 | 70 | **120** | 46 | 258 | **380** | 145 | 1495 | **1675** | 638 | This work |
| MOF-210 | 86 | **176** | 44 | 264 | **475** | 118 | 2396 | **2870** | 712 | This work |
| UMCM-2 | 69 | **124** | 50 | ND | ND | ND | ND | ND | ND | (*S32*) |
| NOTT-112 | 76 | **107** | 54 | ND | ND | ND | ND | ND | ND | (*S33*) |
| PCN-14 | 44 | **67** | 55 | 212* | **222*** | 193* | ND | ND | ND | (*S34*) |
| MIL-101c | ND | ND | ND | 172 | **295** | 130 | 775 | **1054** | 464 | (*S36*) |
| Bulk gas density | NA | NA | 26 | NA | NA | 59 | NA | NA | 131 | (*S38*) |

[‡]Maximum values were used when isotherms show saturation uptake. [†]Crystal density was applied to the gravimetric density. *Measured at 290 K.

**References**


S1. S. B. Choi *et al*., *Cryst. Growth & Des.* **7**, 2290 (2007).

S2. G. Hennrich, *Tetrahedron* **60**, 9871 (2004).

S3. S. Takahashi, Y. Kuroyama, K. Sonogashira, N. Hagihara, *Synthesis* **1980**, 627 (1980).

S4. R. K. Castellano, J. Rebek Jr., *J. Am. Chem. Soc.* **120**, 3657 (1998).

S5. Y. Miura, Y. Yoshida, *Macromol. Chem. Phys*. **203**, 879 (2002).

S6. A. Suzuki, *Pure Appl. Chem*. **66**, 213 (1994).

S7. A. Suzuki, *Chem. Commun*. **2005**, 4759 (2005).

S8. Bruker SMART version 5.625, Area-Detector Software Package; Bruker AXS 1997-2001. Madison, WI, USA.

S9. Bruker SAINT+ version 6.04. SAX Area-Detector Integration Program. Bruker AXS 1997-2001. Madison, WI, USA.

S10. G. M. Sheldrick, SADABS version 2.03, a Program for Empirical Absorption Correction; Universität Göttingen, 1997-2001.

S11. H. K. Chae *et al.*, *Nature* **427**, 523 (2004).

S12. Bruker AXS SHELXTL version 6.10. Structure Determination Package. Bruker AXS 2000. Madison, WI, USA.

S13. L. J. Farrugia, *J. Appl. Cryst.* **32**, 837 (1999).

S14. Materials Studio v 4.0. Accelrys Software Inc., San Diego, CA 92121, USA.

S15. Bruker APEX2 version 5.053. Bruker AXS Inc., Madison, WI, USA.

S16. A. L. Spek, (2008) PLATON, A Multipurpose Crystallographic Tool, Utrecht University, Utrecht, The Netherlands.

S17. A. J. Arvai, C. Nielsen, ADSC Quantum-210 ADX Program, Area Detector System Corporation; Poway, CA, USA, 1983.

S18. Z. Otwinowski, W. Minor, in *Methods in Enzymology*, ed. C. W. Carter Jr., R. M. Sweet, Academic Press, New York, 1997, vol. 276, part A, pp. 307.

S19. J. Rohlícek, M. Husák, *J. Appl. Cryst*. **40**, 600 (2007).

S20. M. J. Frisch, G. W. T., H. B. Schlegel, G. E. Scuseria, M. A. Robb, J. R. C., J. A. Montgomery Jr., T. Vreven, K. N. Kudin, J. C. B., J. M. Millam, S. S. Iyengar, J. Tomasi, V. Barone, B. M., M. Cossi, G. Scalmani, N. Rega, G. A. Petersson, H. N., M. Hada, M. Ehara, K. Toyota, R. Fukuda, J. H., M. Ishida, T. Nakajima, Y. Honda, O. Kitao, H. Nakai, M. K., X. Li, J. E. Knox, H. P. Hratchian, J. B. Cross, C. Adamo, J. J., R. Gomperts, R. E. Stratmann, O. Yazyev, A. J. Austin, R. C., C. Pomelli, J. W. Ochterski, P. Y. Ayala, K. Morokuma, G. A. V., P. Salvador, J. J.

Dannenberg, V. G. Zakrzewski, S. D., A. D. Daniels, M. C. Strain, O. Farkas, D. K. M., A. D. Rabuck, K. Raghavachari, J. B. Foresman, J. V. O., Q. Cui, A. G. Baboul, S. Clifford, J. Cioslowski, B. B. S., G. Liu, A. Liashenko, P. Piskorz, I. Komaromi, R. L. M., D. J. Fox, T. Keith, M. A. Al-Laham, C. Y. Peng, A. N., M. Challacombe, P. M. W. Gill, B. Johnson, W. C., M. W. Wong, C. Gonzalez, and J. A. Pople,. Gaussian 03; Revision C.02 ed.; Gaussian, Inc.: Wallingford, CT (2004).

S21. C. M. Breneman, K. B. Wiberg, *J. Comput. Chem.* **11**, 361 (1990).

S22. S. L. Mayo, B. D. Olafson, W. A. Goddard, *J. Phys. Chem.* **94**, 8897 (1990).

S23. J. J. Potoff, J. I. Siepmann, *AlChE J.* **47**, 1676 (2001).

S24. H. Frost, T. Düren, R. Q. Snurr, *J. Phys. Chem. B* **110**, 9565 (2006).

S25. K. S. Walton, R. Q. Snurr, *J. Am. Chem. Soc.* **129**, 8552 (2007).

S26. T. Düren, F. Millange, G. Férey, K. S. Walton, and R. Q. Snurr, *J. Phys. Chem. C* **111**, 15350 (2007).

S27. Y-S. Bae, A. Ö. Yazaydin, R. Q. Snurr, *Langmuir* **26**, 5475, 2010.

S28. A. K. Rappe, C. J. Casewit, K. S. Colwell, W. A. Goddard III, W. M. Skiff, *J. Am. Chem. Soc* **114**, 10024 (1992).

S29. A. P. Nelson, O. K. Farha, K. L. Mulfort, J. T. Hupp, *J. Am. Chem. Soc.* **131**, 458 (2009).

S30. C. J. Doonan, W. Morris, H. Furukawa, O. M. Yaghi, *J. Am. Chem. Soc.* **131**, 9492 (2009).

S31. H. Furukawa, M. A. Miller, O. M. Yaghi, *J. Mater. Chem.* **17**, 3197 (2007).

S32. K. Koh, A. G. Wong-Foy, A. J. Matzger, *J. Am. Chem. Soc.* **131**, 4184 (2009).

S33. Y. Yan *et al.*, *Chem. Commun.* **2009**, 1025 (2009).

S34. S. Ma *et al.*, *J. Am. Chem. Soc.* **130**, 1012 (2008).

S35. G. Férey *et al.*, *Science* **309**, 2040 (2005).

S36. P. L. Llewellyn *et al.*, *Langmuir* **24**, 7245 (2008).

S37. S. S. Kaye, A. Dailly, O. M. Yaghi, J. R. Long, *J. Am. Chem. Soc.* **129**, 14176 (2007).

S38. Thermophysical properties of fluid systems. NIST Chemistry Webbook, http://webbook.nist.gov/chemistry/fluid/.